OXFORD
UNIVERSITY PRESS | Brain

Posterior integration and thalamo-frontotemporal broadcasting are impaired in disorders of consciousness

Journal:	*Brain*
Manuscript ID	BRAIN-2021-02387
Manuscript Type:	Original Article
Date Submitted by the Author:	02-Dec-2021
Complete List of Authors:	Panda, Rajanikant; Universite de Liege Faculte de Medecine, GIGA Consciousness; Centre hospitalier universitaire de Liege, Coma Science Group López-González3, Ane; Pompeu Fabra University, Department of Information and Communication Technologies Gilson, Matthieu; Pompeu Fabra University, Department of Information and Communication Technologies; Research Centre Jülich Gosseries, Olivia; Universite de Liege Faculte de Medecine, GIGA Consciousness; Centre hospitalier universitaire de Liege, Coma Science Group Thibaut, Aurore; Universite de Liege Faculte de Medecine, GIGA Consciousness; Centre hospitalier universitaire de Liege, Coma Science Group Frasso, Gianluca; Wageningen Food Safety Research Cecconi, Benedetta; Universite de Liege Faculte de Medecine, GIGA Consciousness; Centre hospitalier universitaire de Liege, Coma Science Group Escrichs, Anira; Pompeu Fabra University, Department of Information and Communication Technologies Deco, Gustavo; Pompeu Fabra University, Department of Information and Communication Technologies; Pompeu Fabra University, Institució Catalana de la Recerca i Estudis Avançats (ICREA); Max Planck Institute for Human Cognitive and Brain Sciences; Monash University Laureys, Steven; University of Liege Faculty of Medicine, GIGA-Consciousness; Centre hospitalier universitaire de Liege, Coma Science Group; Laval University, CERVO Research Center Zamora-López, Gorka; Pompeu Fabra University, Department of Information and Communication Technologies Annen, Jitka; Universite de Liege Faculte de Medecine, GIGA Consciousness; Centre hospitalier universitaire de Liege, Coma Science Group
Methodology:	NEUROBIOLOGY OF DISEASE
Subject area:	NEUROONCOLOGY, TRAUMATIC BRAIN AND SPINAL CORD INJURY, NEUROPATHY, OTHER

SCHOLARONE™
Manuscripts

Posterior integration and thalamo-frontotemporal broadcasting are impaired in disorders of consciousness

Rajanikant Panda[1,2]*, Ane López-González[3]*, Matthieu Gilson[3,4], Olivia Gosseries[1,2], Aurore Thibaut[1,2], Gianluca Frasso[5], Benedetta Cecconi[1,2], Anira Escrichs[3], Gustavo Deco[3,6,7,8], Steven Laureys[1,2,9], Gorka Zamora-López[3#], Jitka Annen[1,2#]

*These Author Contributed Equally

#These authors share supervision

Abstract:

The study of the brain's dynamical activity is opening a valuable source of assistance for the clinical diagnosis of patients with disorders of consciousness. For example, dysfunctional spread of naturalistic and synthetic stimuli has proven useful to characterize hampered consciousness. However, understanding of the mechanisms behind loss of consciousness following brain injury is still missing. Here, we study the propagation of endogenous and *in-silico* exogenous perturbations in patients with disorders of consciousness, based upon directed and causal interactions estimated from resting-state fMRI. We found that patients with disorders of consciousness suffer decreased capacity for neural propagation and responsiveness to events. Particularly, that loss of consciousness is related to the malfunctioning of two neural circuits: the posterior cortical regions failing to convey information, in conjunction with reduced broadcasting of information from subcortical, temporal, parietal and frontal regions. These results seed light on the mechanisms behind disorders of consciousness, thus opening new possibilities for clinical applications.

Author affiliations:

[1]Coma Science Group, GIGA-Consciousness, University of Liege, Liege, Belgium

[2]Centre du Cerveau, University Hospital of Liege, Liege, Belgium

[3]Computational Neuroscience Group, Center for Brain and Cognition, Department of Information and Communication Technologies, Pompeu Fabra University, Barcelona, Spain.

1

1   [4]Institute of Neuroscience and Medicine (INM-6) and Institute for Advanced Simulation (IAS-6)

2   and JARA Institute Brain Structure-Function Relationships (INM-10), Jülich Research Centre,

3   Jülich, Germany.

4   [5]Wageningen Food Safety Research, Akkermaalsbos 2, 6708WB, Wageningen, Netherlands

5   [6]Institució Catalana de la Recerca i Estudis Avançats (ICREA), Barcelona, Catalonia, Spain.

6   [7]Department of Neuropsychology, Max Planck Institute for Human Cognitive and Brain Sciences,

7   Leipzig, Germany.

8   [8]School of Psychological Sciences, Monash University, Melbourne, Clayton VIC 3800, Australia.

9   [9]CERVO Research Center, Laval University, Canada

10

11   Corresponding author:

12   Rajanikant Panda

13   Coma Science Group, GIGA-Consciousness, University of Liege, Liège, Belgium

14   Email: rajanikant.panda@uliege.be

15   Ane López-González

16   Center for Brain and Cognition, Pompeu Fabra University, Barcelona, Spain.

17   Email: ane.lopez@upf.edu

18   **Running title:** integration-broadcasting impaired in DOC

19   **Keywords:** disorders of consciousness, *in-silico* exogenous perturbations, receiving information,

20   broadcasting of information,

21   **Abbreviations:** BOLD = Blood oxygenation level dependent; CRS-R = Coma Recovery Scale-

22   Revised; DOC = Disorders of consciousness; EC = effective connectivity; FDG-PET = Fluoro-

23   deoxyglucose Positron Emission Tomography; fMRI = functional MRI; HC = Healthy control;

24   MCS = Minimally conscious state; MOU = multivariate Ornstein-Uhlenbeck; PCC = Posterior

25   cingulate cortex; UWS = Unresponsive wakefulness syndrome; SC = structural connectivity; τ =

26   Relaxation time constants;

27

28

2

1 **Introduction**

2   Consciousness is a subjective experience. Internally perceived as the personal experience of
3 "*what is it like, to be you*", the definition of consciousness and its origin are still a matter of
4 scientific and philosophical debates without consensus.[1–4] Within the clinical context, however,
5 practitioners treating patients with severe brain injuries and disorders of consciousness (DOC) face
6 the daily reality to help their patients in the best possible manner, regardless of the exact definition
7 of consciousness. Therefore, it is important to count with tangible and measurable correlates of
8 consciousness in order to accurately assess the state of the patients at the behavioral level. The use
9 of neuroimaging proxies can thus improve diagnosis and decision making, and contribute to
10 clarifying the mechanisms behind pathological loss of consciousness.[5]

11   Behavioral assessment such as the response to sensory stimuli, pain or simple commands is
12 the first line of action taken at bedside. From this perspective, it has proven useful to characterize
13 consciousness based upon two components: wakefulness (the level of arousal) and awareness (the
14 content of consciousness)[6,7] Patients with severe brain injury can fall into a coma, which is
15 characterized by the absence of both wakefulness and awareness. Patients surviving coma often
16 recover signs of wakefulness, i.e. eye opening, but without manifestation of awareness of the self
17 nor of the environment. Such state is known as unresponsive wakefulness syndrome (UWS) or
18 vegetative state.[6] Some of these patients gradually regain awareness and progress into the so-called
19 minimally conscious state (MCS), showing a wider range of non-reflexive behaviors such as visual
20 pursuit, localization to pain or response to simple commands, although their ability to functionally
21 communicate remains hampered.[8]

22   An upcoming approach to assess brain states in the clinical environment relies on the analysis
23 of the brain's dynamical activity. It is well-known that neural activity is characterized by different
24 frequency bands across sleep stages[9] or cognitive circumstances, and that local field potentials
25 display intercalated epochs of bursting activity followed by silent periods during anesthesia.[10]
26 Recent studies have shown that loss of consciousness leads to reduced spontaneous neural
27 activity[11] and metabolism,[12,13] and that functional connectivity between brain or cortical regions is
28 also significantly reduced.[7,13,14] Moreover, the fluctuating patterns of functional connectivity are
29 altered during reduced consciousness, with shorter life-times and more random transitions between
30 the patterns as observed in normal awake.[14–17]

1   Observing how external perturbations propagate through the brain constitutes an indirect

2   window to probe the brain dynamics, and thus its state. For example, natural audio-visual stimuli

3   presented to subjects undergoing general anesthesia or within deep sleep are still processed in the

4   sensory cortices but fail to integrate at the higher level cortical regions.[18,19] Application of artificial

5   perturbations such as transcranial magnetic stimulation triggers a response of the stimulated

6   regions that is comparable in all cases, but a rapid decline in the propagation of the signals is found

7   during deep sleep, anesthesia or patients with DOC.[20,21] These observations have been successfully

8   employed to classify the level of consciousness both in patients and during anesthesia.[21] However,

9   as the procedure focuses on the description of the whole-brain responses by a single number – the

10   perturbational complexity index, it misses the directionality of the evoked causal interactions.

11   These causal interactions have been demonstrated to be sensitive to different states of

12   consciousness and moreover to hold explanatory power with respect to their neural

13   mechanisms.[22,23]

14   In the present paper, we investigate the capacity of both endogenous and exogenous events to

15   propagate along the brain in patients with disorders of consciousness as compared to normal

16   wakefulness. By use of model-free and model-based analysis methods, all relevant information to

17   characterize the potential of stimuli to propagate is extracted from the resting-state activity, as

18   measured via functional MRI. Thus, bypassing the need to carry out clinical stimulation protocols.

19   First, we studied how spontaneous endogenous events observed within the resting-state Blood

20   oxygenation level dependent (BOLD) propagate and are subsequently integrated.[24] We found that

21   the autocovariance relaxation times of the BOLD signals exhibit a spatial distribution in healthy

22   controls which was disrupted in DOC patients, especially in the UWS group, followed by a

23   significantly reduced capacity to integrate endogenous events. Then, we employed a model-based

24   approach to estimate the effective connectivity between pairs of brain regions.[25–27] Since effective

25   connectivity captures the directional causal relations, we could simulate the asymmetrical

26   propagation of exogenous perturbations on the network in order to identify feedforward and

27   backward effective pathways, and to recognize changes in the ability of brain areas to 'broadcast'

28   or to 'receive' information. In particular, we found two well-differentiated subnetworks with

29   altered propagation properties in the patients. The posterior regions of the cortex fail to convey

30   information, while broadcasting of information is reduced in subcortical, temporal, parietal and

4

1 frontal regions. These results evidence that patients with prolonged disorders of consciousness

2 lack of the capacity for the integration of events that would lead to conscious perception.

3

Materials and methods

Participants

6 We included subjects with a pathological reduction or loss of consciousness after severe brain

7 injury, so called disorders of consciousness (DOCs), as well as healthy control (HC) volunteers.

8 Written informed consent was obtained from all HC participants and the legal representative of

9 DOC patients for participation in the study. The local ethics committee from the University

10 Hospital of Liège (Belgium) approved the study. Forty adult DOC patients, in which 26 in

11 minimally conscious state (MCS) (7 females, age range 23-73 years; mean age ± SD, 41 ± 13

12 years) and 14 with the unresponsive wakefulness syndrome (UWS) (7 females, age range 20-74

13 years; mean age ± SD, 49 ± 16 years) and 33 age and gender matched HC (13 females, age range

14 19-72 years; mean age ± SD, 40 ± 14 years) without premorbid neurological problems were

15 included.   The diagnosis of the DOC patients was confirmed through two gold standard

16 approaches. The first is the repeated behavioral assessment using the Coma Recovery Scale-

17 Revised (CRS-R) by trained clinicians and the second used Fluoro-deoxyglucose Positron

18 Emission Tomography (FDG-PET) neuroimaging as an objective test to complement behavioral

19 assessment according to the procedure described by Stender et al.[12] Patients for whom these two

20 diagnostic approaches disagreed were excluded from further analysis. Patients were behaviorally

21 diagnosed through the best of at least 5 CRS-R assessments, evaluating auditory, visual, motor,

22 oromotor function, communication and arousal.[46] Patient specific clinical information is presented

23 in Supplementary Table 1.

MRI Data Acquisition

25 Structural (T1 and Diffusion Weighted Imaging, DWI) and functional MRI (fMRI) data was

26 acquired on a Siemens 3T Trio scanner. The 3D T1-weighted MP-RAGE images (120 transversal

27 slices, repetition time = 2300 ms, voxel size = 1.0 x 1.0 x 1.2 mm3, flip angle = 9°, field of view

5

1   = 256 x 256 mm2) were acquired prior the 10 minutes of BOLD fMRI resting state (i.e., task free)

2   acquisition (EPI, gradient echo, volumes = 300, repetition time = 2000 ms, echo time = 30 ms, flip

3   angle = 78°, voxel size = 3 x 3 x 3 mm3, field of view = 192×192 mm2, 32 transversal slices).

4   Last, diffusion weighted MRI was acquired in 64 directions (b-value =1,000 s/mm2, voxel size =

5   1.8x1.8x3.3 mm3, field of view 230x230 mm2, repetition time 5,700 ms, echo time 87 ms, 45

6   transverse slices, 128x128 voxel matrix) preceded by a single unweighted image(b0).

MRI data preprocessing

8   Preprocessing was performed using MELODIC version 3.14, which is part of FMRIB's Software

9   Library (FSL, http://fsl.fmrib.ox.ac.uk/fsl). The preprocessing consisted of the following steps:

10   motion correction, non-brain tissue removal, intensity normalization, temporal band-pass filtering,

11   spatial smoothing, rigid-body registration and single-session ICA. Then noise components and

12   lesion-driven artifacts were manually regressed out for each subject using FIX.[47] Subsequently,

13   the Shen et al (2015) functional resting state atlas (without cerebellum) was used for parcellation

14   to obtain the BOLD time series of the 214 cortical and subcortical brain areas in each individual's

15   native EPI space.[48] Finally, he atlas from MNI space to the single-subject functional data and time

16   series for each of the 214 brain areas were extracted.

17   We also computed an average whole-brain structural connectivity matrix from all healthy

18   participants as described in our previous study.[17] Briefly, probabilistic tractography was calculated

19   in native diffusion space using the default PROB-TRACKX settings[49] to estimate the connectivity

20   probability of each brain area to each of the other 213 brain areas. Subsequently, to obtain the

21   structural probability matrix, the value of each brain area was divided by its corresponding number

22   of generated tracts. Finally a group structural connectivity (SC) mask was obtained by averaging

23   the all HC subjects' SC matrix and applying a threshold of 80% to maintain the top 20% of

24   strongest connections to binarize the SC. This SC mask was used to constrain the functional

25   connectivity matrix for the whole brain EC computation (See Supplementary Material for details).

Data Analysis

Intrinsic Ignition

6

1 Intrinsic ignition describes the influence of local endogenous events – spontaneously occurring –

2 over the whole-brain network and their subsequent integration.[24] See Deco et al. (2017) for

3 details.[24] Local events are defined as significantly large fluctuations taking place in the resting-

4 state BOLD signals. First, the BOLD signals were transformed into z-scores, $Z_i(t)$, and binarized

5 by imposing a threshold θ such that the binary signal takes value 1 if $Z_i(t) > \theta$ and 0 otherwise.

6 Here we considered θ = 2 standard deviation. For every endogenous event identified, we calculated

7 the subsequent integration of the event by the network. The phase-locking matrix of the network

8 (See Supplementary Material for details) was calculated for a time-window of 4TR post-event.

9 Phase-locking matrices account for the instantaneous level of pairwise synchronization, see below.

10 Integration is then calculated as the area-under-the curve delimited by the size of the largest

11 component in the binarised phase-locking matrix, for all thresholds from 1 to 0. The mean intrinsic

12 ignition is finally calculated as the average integration triggered by all events occurring in the

13 resting-state BOLD for a subject. Higher values of intrinsic ignition correspond to rich and flexible

14 brain dynamics whereas lower values correspond to poor and rigid, structurally driven brain

15 dynamics.

16 **Relaxation time constants (τ)**

17 In order to obtain information about the operating regime of brain regions, we measured the

18 relaxation time constant τ from the BOLD signals. Specifically, we measured the time constant of

19 the autocovariance for each brain region individually, using time shifts from 0 to 1 TRs. Given

20 that $\hat{Q}_{ij}^0$ and $\hat{Q}_{ij}^1$ are the zero-lag and 1TR-lag covariance matrices from the empirical BOLD, the

21 time constants τ_i are calculated as:

22
$$\tau_i = -\frac{1}{a(v_i|u)},$$

23 where $a(v_i|u)$ corresponds to the slope of the linear regression of $v_i = [log\left(\hat{Q}_{ij}^0\right), \hat{Q}_{ij}^1]$ by u=[0,1].

24 Apart from the information extracted out of the regional time constants, the calculated τ_i were also

25 employed to inform the estimation of effective connectivity.[26]

26 **Estimation of effective connectivity**

1   We estimated whole-brain effective connectivity from the resting-state BOLD signals considering

2   the multivariate Ornstein-Uhlenbeck (MOU) process as the generative dynamical model of the

3   BOLD.[25,27] See Gilson et al (2016) for details.[25] The MOU is a model of Gaussian noise diffusion

4   on a network that has been popular to study the relation between the anatomical connectivity and

5   the whole-brain network dynamics.[25] Given a structural connectivity matrix **A**, the MOU is defined

6   as:

7
$$dx_i = \left(-\frac{x_i}{\tau_i} + A_{ij}x_j \right)dt + dB_i,$$

8   where x_i corresponds to the activity (BOLD signal) of a brain region i, τ_i is the time constant

9   characterizing the exponential decay and dB is a colored noise given by a covariance matrix Σ.

10   The zero-lag Q^0 and 1TR-lag Q^1 covariance matrices of this model can be analytically calculated.

11   The model is thus fitted to empirical data by a Lyapunov optimization procedure such that the

12   distance between the empirical and the estimated Q^0 and Q^1 covariances is minimized[25] The

13   optimization process was initialized considering **A** as the binarized structural connectivity matrix

14   in order to restrict the optimization to links identified via diffusion imaging. The estimations were

15   performed using the pyMOU python package.

16   ### *In-silico* exogenous perturbational analysis

17   Considering the MOU as the generative dynamical model for the diffusion of noise in a network,

18   the network responses to local perturbations can be analytically estimated; see Gilson et al.

19   (2019).[26] In particular, we characterise the Green function of the MOU for a given connectivity

20   matrix A. The Green function describes the temporal network responses at times t > 0, due to a

21   unit perturbation applied at a given brain region i at time t = 0. For the MOU process, the

22   spatiotemporal responses are given by:

23
$$R(t) = \|J^0\|\left(e^{Jt} - e^{J^0 t}\right),$$

24   where J is the Jaccobian of the MOU process, $J_{ij} = -\frac{\delta_i}{\tau} + A_{ij}$ and $J_{ij}^0 = -\frac{\delta_{ij}}{\tau}$ is the Jaccobian

25   associated to the leakage term alone, characterising the decay rate of the system. $\|J^0\|$ is a

26   normalization term to make analysis across networks comparable. The response matrices $R(t)$

1   encode the spatio-temporal responses to nodal perturbations. In other words, a pair-wise element

2   $R_{ij}(t)$ represents the temporal response of area j to a unit perturbation applied on area i at time t =

3   0. This conditional, pair-wise response encompases all network effects from i to j acting at different

4   time scales. Note that in Ref. Gilson et al., (2019)[26] the network responses $R(t)$ were referred to

5   as 'dynamic communicability $C(t)$'. Here we adopted a nomenclature that is clearer and

6   conceptually more precise in order to facilitate the interpretation of results.

7   As in Ref. Gilson et al. (2019),[26] in the present study, the connectivity matrices **A** are the effective

8   connectivity matrices previously estimated for each subject. Hence, the propagation of responses

9   to exogenous perturbations are constrained by the strength of the directed, causal interactions

10 between every pair of brain regions.

11 The global network response $r(t)$ is the sum of all pairwise responses at each time point:

12
$$r(t) = \sum_{i,j=1}^{N} R_{ij}(t),$$

13 accounting for the total excitability of a network to exogenous perturbation.

14 Since effective connectivity estimates the directed, causal pairwise interactions between brain

15 regions, and the response matrices $R(t)$ are constrained upon effective connectivity, $R(t)$ account

16 for the asymmetric interactions between brain regions. The broadcasting capacity of a region i is

17 calculated as the sum of all responses exerted by region i on the rest of brain areas, and the

18 receiving or integration capacity is given by the sum of responses elicited on region i, by the

19 perturbations at all areas. That is, the broadcasting and receiving capacities of a node are calculated

20 as the row and column sum of the response matrices $R(t)$ at each time point t:

21
$$\text{Broadcasting capacity: } r_i^+(t) = \sum_{j=1}^{N} R_{ij}(t), \text{ and}$$

22
$$\text{Receiving capacity: } r_i^-(t) = \sum_{j=1}^{N} R_{ij}(t).$$

23 Note that in Refs. Gilson et al. (2019)[26] the broadcasting and receiving capacities are referred to

24 as out-communicability and in-communicability respectively.

9

Statistical analysis

For the model free measure, two-sample t-tests were used to assess group differences in global Intrinsic Ignition and relaxation time constant τ at the whole brain level (Bonferroni correction for 3 groups). Then we investigated local between group differences in regional relaxation time constant τ using two-sample t-tests with Bonferroni correction ($p<0.05$) accounting for the number of regions (i.e., N = 214).

For the model free measure, first, we assess between group differences for the EC links using two-sample t-tests with Bonferroni correction ($p<0.05$) accounting for the number of regions (i.e., N = 214) and structural link threshold. Second, we assess between group differences in whole-brain total (i.e., receiving and broadcasting) communicability. An ANOVA with Tukey post hoc comparison, Bonferroni corrected for 200 timepoints of integration, was employed. Third, to investigate local broadcasting and receiving properties, we considered the area under the receiving and broadcasting curves separately for every brain region. We identified regions with relatively high communicability within groups (i.e., the different states within the DOC) with a one-sample t-test with FDR <0.05 correction for the number of regions (i.e., N = 214). Last, between group differences in regional receiving and broadcasting information were assessed with two-sample t-tests. Between group statistics were corrected using Bonferroni correction ($p<0.05$) accounting for the number of regions (i.e., N = 214).

Data Availability

The multimodal neuroimaging data used in this experiment are available upon request with appropriate procedures. After the acceptance of the manuscript, the code used for this study will be available at: https://github.com/RajanikantPanda/Ignition_and_Information_flow_for_DOC

Results

This study comprises resting-state fMRI (eyes-closed) of 33 healthy control (HC) subjects, 14 patients with unresponsive wakefulness syndrome (UWS) and 26 patients classified as in

1   minimally conscious state (MCS). The diagnoses were made using repeated CRS-R assessments

2   and confirmed with FDG-PET neuroimaging[12] to avoid including MCS* patients.[13]

Global integration of local endogenous events is hampered in lower conscious states

5   We started this study by investigating whether endogenous spontaneous events occurring

6   locally propagate differently depending on the level of consciousness, across healthy controls,

7   MCS patients or patients with UWS. For that, we employed the *intrinsic ignition* measure.[24] The

8   level of global integration for a subject is calculated as the average integration triggered by all

9   endogenous events identified in their resting-state BOLD session, see Methods. As shown in **Fig.**

10 **1a**, the mean intrinsic ignition was lowest in UWS patients implying that the endogenous BOLD

11 events lead to a lower network response than in healthy controls and in MCS patients (HC =

12 0.81±0.01, UWS = 0.78±0.01, MCS = 0.79±0.01, HC vs. UWS t(45)=6.6, p<0.0001, HC vs. MCS

13 t(57)=4.6, p<0.0001, MCS vs. UWS t(38)=2.3, p=0.012). It shall also be noted that the number of

14 observed intrinsic events was lowest in UWS patients, intermediate in MCS patients and highest

15 in healthy controls (HC = 14.1±3.6, UWS = 7.6±2.9, MCS = 11.0±3.6, HC vs. UWS t(45)=5.9,

16 p<0.0001, HC vs. MCS t(57)=3.3, p=0.0017, MCS vs. UWS t(38)=2.9, p=0.0048).

Shorter relaxation-time of BOLD signals in low levels of consciousness

19 Measuring time-scales from signals – i.e, multivariate time-series – can reveal changes in the

20 underlying mechanisms controlling the local dynamics and determining their operating regime.

21 Specifically, the autocovariance profile of the BOLD signal for each brain area measures the

22 duration for which the signal is altered before going back to pre-event baseline activity.[28] Here,

23 we measure the autocovariance time constant τ, also called the relaxation time or memory depth

24 in the literature. Large τ implies a longer lingering effect of a signal after an event or perturbation

25 before it decays, thus suggesting that the brain region might remain available for processing longer.

26 At a whole-brain level, averaging over the τ_i for all regions in one subject, we found that τ

27 was smaller in UWS patients (1.96±0.38) than in healthy controls (2.72±0.35; t(45)=6.5,

11

1   p<0.0001) and MCS patients (2.70±0.58; t(38)=4.2, p<0.001), see **Fig. 1b**. Looking at the region-

2   wise spatial distributions, we found that in healthy controls τ_i is heterogeneously distributed

3   showing a gradient with shorter time constants in subcortical areas ($\tau_i \sim 1.5$ sec) and longer (τ_i

4   ~3.5 sec) in the frontal and in the parietal areas, see **Supplementary Fig. 1**. Importantly, the

5   diversity of relaxation times is lost in the UWS patients with τ_i being homogeneously distributed

6   and dominated by small values. Compared to healthy controls, the decrease of τ_i in UWS patients

7   was most predominant in the bilateral thalamus, right caudate, left hippocampus,

8   parahippocampus, bilateral posterior, middle and anterior cingulate, insula, inferior, middle,

9   superior and dorsolateral frontal areas, **Fig. 1c and Supplementary Table 2**. In the case of MCS

10   patients the heterogeneity of τ_i distribution was practically recovered, **Supplementary Fig. 1**.

11   Compared to the healthy controls, in MCS patients τ_i was lower only in the bilateral thalamus and

12   left medial prefrontal cortex, see **Fig. 1d and Supplementary Table 2**.

13   So far, the results obtained for the intrinsic ignition and the distribution of relaxation time

14   constants from the resting-state BOLD signals indicate a breakdown in the signals' spatiotemporal

15   structure that involves reduced propagation and integration capabilities of endogenous events in

16   DOC patients, especially in the UWS group. For the remaining of the paper we shift to model-

17   based analyses.

18   **Whole-brain effective connectivity shows altered causal interactions**

19   **in DOC patients**

20   In order to identify alterations to the causal relations between the brain regions, we estimated

21   whole-brain effective connectivity (EC) from the resting-state BOLD for each subject. The

22   estimation of EC considers a model of Gaussian noise diffusion – the multivariate Ornstein-

23   Uhlenbeck – on top of the anatomical connectivity as the generative dynamics[25,27] in order to

24   capture the origin of the fluctuations in the BOLD; see **Fig. 2a** and Methods for further details. In

25   short, EC estimation consists of identifying the most likely causal interactions that give rise to the

26   observed BOLD signals, fitting both the interaction strengths between all pairs of ROIs and the

27   levels of noise to stimulate each ROI, **Fig. 2a**.

28   At the whole-brain level, averaging across all EC links, we found that the EC of the UWS

29   patients was higher than for the healthy controls or in MCS patients (HC = 0.015±0.002, UWS =

12

1 0.019±0.004, MCS = 0.014±0.003; HC vs. UWS t(45)=-4.7, p<0.0001, MCS vs. UWS t(38)=-4.0,

2 p<0.001). A closer inspection of the pair-wise EC values revealed the presence of links that either

3 increased or decreased in the UWS patients in respect to the healthy controls, **Fig. 2b**. The UWS

4 patients showed increased EC for connections between subcortical and cortical regions (thalamus,

5 caudate and putamen), but decreased EC in connections spanning posterior (i.e., parietal, occipital)

6 to frontal (i.e., temporal and frontal) regions as well as between midline posterior regions (parietal,

7 occipital) and middle frontal regions. The MCS patients showed especially lower EC in

8 interactions from posterior to frontal and temporal regions and midline regions encompassing the

9 middle prefrontal and posterior cortex and the thalamus, see **Fig. 2c**, including regions important

10 for long range connectivity and overlapping with key areas of the Default Mode Network.

Altered spatiotemporal propagation of exogenous perturbations

12 Having identified changes in specific pair-wise EC connections for both UWS and MCS

13 patients, the question is now how do those alterations affect the propagation of information in the

14 brain. To answer this question, we perform an *in-silico* perturbational study to assess how

15 exogenous perturbations, applied to individual ROIs, spread along the network. Considering the

16 same generative dynamical model as for the EC estimation, the effect of regional perturbations on

17 the rest of the network can be analytically estimated,[26] see Methods. The spatiotemporal responses

18 of nodal perturbations are encoded into the temporal response matrices R(t). The evolution of

19 response matrices for the three study cases are shown in **Fig. 3a**. Specifically, a pair-wise element

20 $R_{ij}(t)$ represents the temporal response of area j to a unit perturbation applied on area i at time t =

21 0. This conditional, pair-wise response encompasses all network effects from i to j acting at

22 different time scales.

23 **Figure 3a** illustrates how the patterns of responses are progressively reshaped over time for

24 the three study groups – healthy controls, UWS patients and MCS patients. The global brain

25 responses (sum over all pair-wise responses) are shown in **Fig. 3b**. As seen, the global responses

26 undergo a transient peak short after the initial perturbations and then decay as the effects of the

27 stimuli dilute with time and the system relaxes back to its stationary state. This relaxation is also

28 observed by the homogenization of the response matrices at the longer latencies in **Fig. 3a**. The

29 global response curves for controls and MCS groups follow quite a similar behavior, both peaking

30 at 18.2±2.9 and 15.6± 3.7 seconds respectively and taking peak values 0.30±0.03 and 0.28± 0.05.

13

1   In the UWS patients, however, the global response peaks sooner (10.6±2.9 sec) (HC vs. UWS

2   t(45)=8.2, p<0.0001, HC vs. MCS t(57)=3.0, p=0.0036, MCS vs. UWS t(38)=4.3, p < 0.001) and

3   displays a higher peak (0.34±0.05) (HC vs. UWS t(45)=-3.3, p= 0.0019, MCS vs. UWS t(38)=-

4   3.1, p = 0.0031) than for the controls and MCS groups, but then it decays notably faster.

5   Quantitatively, we found that the area-under-the-curve in the time spanning 60-200 sec (modeled

6   time) significantly decreases for the UWS group (0.08±0.06) and MCS patients (0.15± 0.04)

7   compared to healthy controls (0.18±0.02) (HC vs. UWS t(45)=7.1, p<0.0001, HC vs. MCS

8   t(57)=2.9, p=0.005, MCS vs. UWS t(38)=3.6, p < 0.001).

9 Broadcasting and integrative capabilities of brain regions across
10 states of consciousness

11   Since EC identifies the directed causal interactions between the brain regions, this allows us

12   to study the input and output relations for each area in respect to the exogenous perturbations. The

13   row sum of the response matrices $\mathbf{R}$(t) represent the broadcasting capacity of a region (i.e., the

14   response that a perturbation in one region elicits on all other areas) and the columns describe the

15   integrative capacity of the brain region (i.e., how much is a region affected by the perturbations

16   applied to all other areas).[26]

17   **Figure 4** reveals that the three levels of consciousness are characterized by distinct spatial

18   distributions of 'broadcaster' and 'receiver' (i.e., integrator) areas. Notably, in UWS patients no

19   brain region stands out either as broadcaster or as integrator, except for the thalamus displaying

20   relatively large receiving capacity. In the healthy controls, we found several regions with both

21   significant broadcasting and receiving capacity: the bilateral occipital, calcarine, lingual, cuneus,

22   precuneus, superior and inferior parietal, right superior temporal. Significant broadcasting-only

23   capacity was found in the bilateral inferior, middle and superior temporal, right parahippocampal,

24   putamen, bilateral insula, inferior parietal, supramarginal, precuneus, middle cingulum and right

25   inferior frontal areas. On the other hand, the bilateral posterior cingulate cortex (PCC), precuneus,

26   supramarginal gyrus, thalamus, middle cingulate, left anterior cingulate and right inferior frontal

27   cortex displayed significant receiving-only capacity. The MCS patient group was characterized by

28   globally reduced broadcasting and receiving properties compared to healthy controls, however

29   they showed a relatively preserved receiving and broadcasting of information within bilateral

14

occipital, cuneus, left calcarine, bilateral superior and inferior parietal, supramarginal, precuneus and the right PCC. Additionally, they presented preserved broadcasting properties in the bilateral middle temporal, postcentral, right calcarine and left inferior frontal cortices, and preserved receiving capacity in the bilateral thalamus, see **Fig.4 and Supplementary Table 3**.

We ended our perturbative analysis by comparing the region-wise group differences of the patients in respect to the healthy controls, which are shown in **Fig. 5**. Following the severely hampered broadcasting and integrating capacity in UWS, reduced information broadcasting in UWS patients as compared to healthy controls was especially notable at the bilateral hippocampus, parahippocampus, thalamus, caudate, amygdala, putamen, insula, inferior/middle temporal, temporal pole, right superior temporal, fusiform, lingual, calcarine, occipital, anterior cingulate, right inferior and middle frontal cortices. The notorious lack of broadcasting capacity of the subcortical regions evidences a reduced activity of the whole network. A profound reduction of the capacity to receive information in the UWS patients compared to the healthy controls was found at the bilateral precuneus, PCC, lingual, calcarine, fusiform, middle occipital, middle / anterior cingulum, inferior / superior parietal, supramarginal, middle temporal, inferior frontal cortices and the middle prefrontal cortex. These regions encompass primary visual and auditory areas, but also higher integration areas in the PCC that have an important hub function within the whole-brain network, see **Fig.5 and Supplementary Table 4**.

The MCS patients showed a less pronounced picture of impaired information in- and out-flows. Compared to healthy controls they showed a significant reduction in the potential to broadcast information in the bilateral thalamus, parahippocampus, left hippocampus, bilateral insula, inferior / middle temporal, right superior temporal, bilateral fusiform and lingual cortices. A reduced capacity to receive information at the bilateral precuneus, PCC, cuneus, right lingual, calcarine, bilateral middle cingulum and right middle temporal cortices. Finally, compared to MCS patients, UWS patients showed additional significant reduction in receiving and broadcasting of information at the left precuneus, occipital cortex, temporal and right superior parietal, thus indicating that the information flow in these areas might be the most important contributors to conscious information processing.

In summary, our model-based analysis to estimate effective connectivity and to simulate *in-silico* the response to exogenous perturbations allowed us to identify specific directed pathways

15

1   that are disrupted in patients with DOC, and thus reveal relevant for the propagation and processing

2   of consciousness.

3

4   # Discussion

5   In the present paper, we have studied the neural propagation of endogenous and exogenous

6   perturbations in the brain using model-free and model-based analysis methods, applied to the

7   problem of elucidating the mechanisms behind loss of consciousness due to acquired brain injury.

8   The methods here employed add significant value to the dynamical approaches for two main

9   reasons. First, they rely on simple observables – the resting-state fMRI – and thus they do not

10   require the execution of experimental exogenous stimulation protocols. And second, unlike

11   previous approaches, they allowed us to investigate the directional causal interactions between

12   brain regions, thus elucidating alterations in the broadcasting and the integrating capacities of

13   individual areas or pathways, between normal awake and unconscious patients. Indeed, our main

14   finding is that we could identify two distinct malfunctioning neural circuits in patients with DOC:

15   the posterior cortical regions fail to convey information, in conjunction with reduced broadcasting

16   of information from subcortical, temporal, parietal and frontal regions. These results show that

17   patients with prolonged disorders of consciousness lack of the capacity for the integration of events

18   that would lead to conscious perception.

19   In healthy controls we found that the relaxation time constants associated with the resting-

20   state BOLD signals display a gradient distribution with shorter relaxation times in subcortical areas

21   and longer time constants in the frontal and in the parietal areas, **Supplementary Fig. 1a.**

22   Accordingly, analysis of exogenous *in-silico* perturbations revealed that the broadcasting of

23   information flow is predominant in a broad range of cognitive modules, including the

24   hippocampus, parahippocampal, temporal, posterior and inferior frontal regions. This subcortical-

25   cortical loop has been proposed to mediate the sensory information to be globally 'accessible' to

26   other cognitive functions through feedforward and feedback loops by the global neuronal

27   workspace theory, and only when access to all cognitive modules occurs, sensory content is

28   elevated to conscious perception.[29–31] Although the activity in the posterior regions is highly

29   influenced by perturbation, suggesting that they have a large cause-effect capacity to receive and

16

1 integrate the information flow, one of the key principles of conscious perception in integration

2 information theory.[1,2,32]

3 Regarding the patients with unresponsive wakefulness syndrome (UWS), the results observed

4 were very much altered. First, the propagation of endogenous events occurring in the resting-state

5 BOLD rapidly decay avoiding their subsequent integration, **Fig. 1a**. This is corroborated by the

6 fact that the spatial distribution of relaxation times fades away in the UWS patients, with all areas

7 taking short relaxation times (**Figs. 1b** and **c**) and evidencing that local activity doesn't properly

8 propagate along the network. Especially frontal, parietal and higher-order cortices which ensure

9 sensory information processing, need longer time to integrate diverse information.[33,34] Second,

10 effective connectivity is reduced overall but interestingly some effective subcortical-cortical

11 connections were found to significantly increase, **Fig. 2b**. The propagation of *in-silico* exogenous

12 perturbations showed a rapid and large response followed by a fast decay, **Fig. 3**, since the

13 information fails to propagate along the network in a sustained manner. Such early hyper-response

14 has been previously seen in UWS patients[35] and in loss of consciousness due to generalized

15 epilepsy possibly caused by excess electrical discharges in the brain.[36] The mechanism for this

16 hyper-response is yet to be elucidated but it could be either due to the network being dominated

17 by short local recurrent loops, or due to a lack of inhibition as in unconscious anesthetized ferrets.[37]

18 Finally, the regional specificities for broadcasting and receiving that were observed in the healthy

19 controls are vanished for the UWS patients. Only the thalamus stands-out, as an area with

20 significant receiving capacity thus probably allowing its gateway function between the body and

21 the brain.

22 The patients in minimally conscious state (MCS) studied here underwent through a coma and

23 a UWS phases after brain injury, but later regained partial consciousness and cognitive

24 functionalities. All the results found for the MCS patients show light alterations to those in the

25 healthy participants, as expected from their partial functional recovery. The spatial gradient of

26 relaxation time constants from the resting-state BOLD is recovered, **Supplementary Fig. 1**, except

27 shorter time constants were still found in the thalamus and the left medial preforntal cortex.

28 Effective connectivity was in general slightly below than those observed in control subjects but a

29 significant reduction was found remaining in fronto-parietal connections and in between temporal

30 regions, **Fig. 2c**. Regional broadcasting and receiving capacities to *in-silico* perturbations

31 displayed a recovered scenario, see **Fig. 4** and see **Supplementary Table 3**. It is clinically relevant

to understand why or how MCS patients could partially recover from the unresponsive wakefulness state. In the light of our results, it seems that an increase in receiving and broadcasting of information at the left precuneus, occipital cortex, temporal and right superior parietal is instrumental for the recovery of conscious information processing, **Fig. 5**

In comparison with healthy controls, the UWS patients showed a reduction of receiving information in posterior regions, which implies sensory information integration is impaired already at the level of sensory regions to the high-level hub regions of the Default Mode Network (i.e. PCC and Precuneus). Indeed, the lack of receiving of information in the sensory areas hampers a stimulus or event to reach awareness, as integration of external inputs is a prerequisite for consciousness.[38] Our results provide a mechanistic explanation for how the ability to receive information in sensory and DMN hub regions alters cerebral information processing, which might be at the essence for the structural and functional anomalies in UWS patients. Although it is known that the PCC and Precuneus have decreased structural, functional and metabolism,[7,12,16,17,39] our results provide a mechanistic explanation that the ability to receive information in sensory and DMN hub regions is reduced in UWS patients. On the other hand, broadcasting was reduced in the subcortical regions (i.e., thalamus, caudate, putamen) and regions involved in higher cognitive function (i.e., temporo-parietal, anterior cingulate and frontal regions). This is aligned with the mesocircuit hypothesis[40] which states that the feedforward connections between these regions play a key role in reaching levels of (cortical) activity that support the stimuli to access consciousness processing. This has been recently confirmed in macaques using invasive-EEG, showing that integration at the thalamus, caudate, putamen and parietal cortex is a hallmark of conscious states.[41] Our findings unravel that human consciousness also relies on the broadcasting capacities from the thalamus, caudate and putamen leads to support the transmission of activity, functional integration and recurrent activity between subcortical and cortical neurons, all of which is lost in UWS patients. Interestingly, we also noted a decrease in receiving and broadcasting capacities in the bilateral temporal areas for DOC patients. Recent studies also noted altered structural[42] and functional loss in the temporal area in DOC patients.[7,13] To date, there is limited explanation for the involvement of the temporal cortex in consciousness. We speculate that a lesser involvement of the temporal areas in the information pathways could impede self-awareness and memory.

Our *in-silico* pertubational study revealed transient global changes to the dissemination of information that are similar to those we observed from the integration of endogenous events with

18

the intrinsic ignition. In DOC patients, and especially in UWS patients, the brain's cause-effect capacity to respond is significantly lower than during normal wakefulness in healthy subjects. It seems that the observed spatiotemporal alterations of local event processing also hamper global integration and whole brain neural responses; as observed both after *in-silico* and endogenous perturbations. These results are in line with empirical studies using TMS, in which the recruitment of global neural activity after perturbation, both in space and time, has been found to be reduced during deep sleep, anesthesia and in DOC.[20,21] In conclusion, the cerebral capacity of propagation and integration of local, naturally occurring events into the entire network is affected by reduced states of consciousness and shares similarities with both information integration theory[1,2] and global neuronal workspace theory.[30,31] Although these theories have distinct concepts of consciousness, our results suggest that they might represent two sides of the same coin.[43–45]

Acknowledgements

19

8   Authors' contributions

9   RP, ALG, JA, GZL, MG, GD and SL designed research. JA and GZL supervised the research. JA,

10   AT, CM, OG and the Coma Science Group Collaborators acquired the data. RP, ALG and AE

11   preprocessed the data. RP, ALG, JA and GF analyzed the data. MG and GZL designed the

12   computational model and optimized the code as per this research study. RP, JA, ALG and GZL

13   wrote the manuscript. All authors interpreted the results and contributed to the editing of the

14   manuscript.

15   Competing interests

16   All the authors report no competing interests.

17   Collaborators

18   Alice Barra, Charlotte Martial, Claire Bernard, Etelle Bonin, Emilie Szymkowicz, Jean-Flory

19   Luaba Tshibanda, Leandro Sanz, Marie Vitello, Roland Hustinx

20   References

21   1.   Tononi G, Boly M, Massimini M, Koch C. Integrated information theory: From

22   consciousness to its physical substrate. *Nat Rev Neurosci*. 2016;17(7).

23   2.   Tononi G. An information integration theory of consciousness. *BMC Neurosci*.

24   2004;5(1):42.

20

1   3.   Nagel T. What Is It Like to Be a Bat? *Philos Rev*. 1974;83(4).

2   4.   Damasio A, Meyer K. Consciousness: An overview of the phenomenon and of its possible
3   neural basis. In: *The Neurology of Consciousness*. ; 2009.

4   5.   Owen AM, Coleman MR. Functional neuroimaging of the vegetative state. *Nat Rev*
5   *Neurosci*. 2008;9(3).

6   6.   Laureys S. The neural correlate of (un)awareness: Lessons from the vegetative state.
7   *Trends Cogn Sci*. 2005;9(12).

8   7.   Demertzi A, Antonopoulos G, Heine L, et al. Intrinsic functional connectivity
9   differentiates minimally conscious from unresponsive patients. *Brain*. 2015;138(9).

10   8.   Laureys S, Owen AM, Schiff ND. Brain function in coma, vegetative state, and related
11   disorders. *Lancet Neurol*. 2004;3(9).

12   9.   Armitage R. The distribution of EEG frequencies in REM and NREM sleep stages in
13   healthy young adults. *Sleep*. 1995;18(5).

14   10.   Silva A, Cardoso-Cruz H, Silva F, Galhardo V, Antunes L. Comparison of anesthetic
15   depth indexes based on thalamocortical local field potentials in rats. *Anesthesiology*.
16   2010;112(2).

17   11.   Wenzel M, Han S, Smith EH, et al. Reduced Repertoire of Cortical Microstates and
18   Neuronal Ensembles in Medically Induced Loss of Consciousness. *Cell Syst*. 2019;8(5).

19   12.   Stender J, Gosseries O, Bruno MA, et al. Diagnostic precision of PET imaging and
20   functional MRI in disorders of consciousness: A clinical validation study. *Lancet*.
21   2014;384(9942).

22   13.   Thibaut A, Panda R, Annen J, et al. Preservation of Brain Activity in Unresponsive
23   Patients Identifies MCS Star. *Ann Neurol*. 2021;90(1).

24   14.   Barttfeld P, Uhrig L, Sitt JD, Sigman M, Jarraya B, Dehaene S. Signature of
25   consciousness in the dynamics of resting-state brain activity. *Proc Natl Acad Sci*.

21

2014;112(3):201418031.

15. Demertzi A, Tagliazucchi E, Dehaene S, et al. Human consciousness is supported by dynamic complex patterns of brain signal coordination. *Sci Adv*. 2019;5(2).

16. Luppi AI, Craig MM, Pappas I, et al. Consciousness-specific dynamic interactions of brain integration and functional diversity. *Nat Commun*. 2019;10(1).

17. López-González A, Panda R, Ponce-Alvarez A, et al. Loss of consciousness reduces the stability of brain hubs and the heterogeneity of brain dynamics. *bioRxiv*. Published online November 22, 2020:2020.11.20.391482.

18. Krom AJ, Marmelshtein A, Gelbard-Sagiv H, et al. Anesthesia-induced loss of consciousness disrupts auditory responses beyond primary cortex. *Proc Natl Acad Sci U S A*. 2020;117(21).

19. Portas CM, Krakow K, Allen P, Josephs O, Armony JL, Frith CD. Auditory processing across the sleep-wake cycle: Simultaneous EEG and fMRI monitoring in humans. *Neuron*. 2000;28(3).

20. Massimini M, Ferrarelli F, Huber R, Esser SK, Singh H, Tononi G. Breakdown of cortical effective connectivity during sleep. supplement. *Science*. 2005;309(5744).

21. Casali AG, Gosseries O, Rosanova M, et al. A theoretically based index of consciousness independent of sensory processing and behavior. *Sci Transl Med*. 2013;5(198).

22. Signorelli CM, Wang Q, Khan I. A compositional model of consciousness based on consciousness-only. *Entropy*. 2021;23(3).

23. Seth AK, Barrett AB, Barnett L. Causal density and integrated information as measures of conscious level. *Philos Trans R Soc A Math Phys Eng Sci*. 2011;369(1952).

24. Deco G, Kringelbach ML. Hierarchy of Information Processing in the Brain: A Novel 'Intrinsic Ignition' Framework. *Neuron*. Published online 2017.

25. Gilson M, Moreno-Bote R, Ponce-Alvarez A, Ritter P, Deco G. Estimation of Directed

22

Effective Connectivity from fMRI Functional Connectivity Hints at Asymmetries of Cortical Connectome. *PLoS Comput Biol*. 2016;12(3).

26. Gilson M, Kouvaris NE, Deco G, et al. Network analysis of whole-brain fMRI dynamics: A new framework based on dynamic communicability. *Neuroimage*. Published online 2019.

27. Adhikari MH, Griffis J, Siegel JS, et al. Effective connectivity extracts clinically relevant prognostic information from resting state activity in stroke. *Brain Commun*. 2021;3(4).

28. Murray JD, Bernacchia A, Freedman DJ, et al. A hierarchy of intrinsic timescales across primate cortex. *Nat Neurosci*. 2014;17(12).

29. Dehaene S, Changeux JP. Experimental and Theoretical Approaches to Conscious Processing. *Neuron*. 2011;70(2).

30. Dehaene S, Changeux JP, Naccache L. The global neuronal workspace model of conscious access: From neuronal architectures to clinical applications. *Res Perspect Neurosci*. 2011;18.

31. Mashour GA, Roelfsema P, Changeux JP, Dehaene S. Conscious Processing and the Global Neuronal Workspace Hypothesis. *Neuron*. 2020;105(5).

32. Oizumi M, Albantakis L, Tononi G. From the Phenomenology to the Mechanisms of Consciousness: Integrated Information Theory 3.0. *PLoS Comput Biol*. 2014;10(5).

33. Yeshurun Y, Nguyen M, Hasson U. Amplification of local changes along the timescale processing hierarchy. *Proc Natl Acad Sci U S A*. 2017;114(35).

34. Hasson U, Yang E, Vallines I, Heeger DJ, Rubin N. A hierarchy of temporal receptive windows in human cortex. *J Neurosci*. 2008;28(10).

35. Di Perri C, Bastianello S, Bartsch AJ, et al. Limbic hyperconnectivity in the vegetative state. *Neurology*. 2013;81(16).

36. Moeller F, Siebner HR, Wolff S, et al. Simultaneous EEG-fMRI in drug-naive children

23

1   with newly diagnosed absence epilepsy. *Epilepsia*. 2008;49(9).

2   37.   Wollstadt P, Sellers KK, Rudelt L, et al. Breakdown of local information processing may
3   underlie isoflurane anesthesia effects. *PLoS Comput Biol*. 2017;13(6).

4   38.   Herbet G, Lafargue G, de Champfleur NM, et al. Disrupting posterior cingulate
5   connectivity disconnects consciousness from the external environment. *Neuropsychologia*.
6   2014;56(1).

7   39.   Annen J, Heine L, Ziegler E, et al. Function–structure connectivity in patients with severe
8   brain injury as measured by MRI-DWI and FDG-PET. *Hum Brain Mapp*. 2016;37(11).

9   40.   Schiff ND. Recovery of consciousness after brain injury: a mesocircuit hypothesis. *Trends
10   Neurosci*. 2010;33(1):1-9.

11   41.   Afrasiabi M, Redinbaugh MJ, Phillips JM, et al. Consciousness depends on integration
12   between parietal cortex, striatum, and thalamus. *Cell Syst*. 2021;12(4).

13   42.   Annen J, Frasso G, Crone JS, et al. Regional brain volumetry and brain function in
14   severely brain-injured patients. *Ann Neurol*. 2018;83(4).

15   43.   Northoff G, Wainio-Theberge S, Evers K. Is temporo-spatial dynamics the "common
16   currency" of brain and mind? In Quest of "Spatiotemporal Neuroscience." *Phys Life Rev*.
17   2020;33.

18   44.   Winters JJ. The temporally-integrated causality landscape: A theoretical framework for
19   consciousness and meaning. *Conscious Cogn*. 2020;83.

20   45.   Northoff G, Lamme V. Neural signs and mechanisms of consciousness: Is there a
21   potential convergence of theories of consciousness in sight? *Neurosci Biobehav Rev*.
22   2020;118.

23   46.   Giacino JT, Kalmar K, Whyte J. The JFK Coma Recovery Scale-Revised: Measurement
24   characteristics and diagnostic utility. *Arch Phys Med Rehabil*. 2004;85(12):2020-2029.

25   47.   Griffanti L, Douaud G, Bijsterbosch J, et al. Hand classification of fMRI ICA noise

24

1   components. *Neuroimage*. 2017;154.

2   48.   Finn ES, Shen X, Scheinost D, et al. Functional connectome fingerprinting: Identifying

3   individuals based on patterns of brain connectivity HHS Public Access Author

4   manuscript. *Nat Neurosci*. 2015;18(11).

5   49.   Behrens TEJ, Woolrich MW, Jenkinson M, et al. Characterization and Propagation of

6   Uncertainty in Diffusion-Weighted MR Imaging. *Magn Reson Med*. 2003;50(5).

7

8   # Figure legends

9   **Figure 1. Changes in endogenous properties from resting-state BOLD signals.** Healthy

10   controls (HC), unresponsive wakefulness syndrome (UWS) and minimally conscious state (MCS)

11   (a) Comparison of mean intrinsic ignition for the three groups, illustrating the reduced capacity to

12   integrate endogenous spontaneous events in patients with DOC. (b) Relaxation time-scales of the

13   BOLD signals (τ) at the whole-brain level shows significant reductions in UWS and MCS patients

14   compared to HC. Stars reflect the Bonferroni corrected (for three groups) significance levels (*=p-

15   value<0.016; **= p-value<0.001; ***= p-value<0.0001). (c,d) Maps of significant differences in

16   regional distributions of τ between patients and controls. The color bar represents the t-values of

17   significant between-group differences (Bonferroni corrected for 214 tests, p-value=0.05).

18   **Figure 2. Comparison of effective connectivity (EC) between healthy controls and patients.**

19   (a) Schematic representation of the fitting procedure leading to estimation of EC. Considering a

20   model of noise diffusion – the multivariate Ornstein-Uhlenbeck process – the whole-brain network

21   model is constrained using structural connectivity obtained from diffusion imaging and then fitted

22   to reproduce the empirical resting-state data. In particular, to fit the zero-lag and 1TR-lag

23   covariance matrices (FC0 and FC1), and the regional noise level Σ_i. (b, c) Maps of significantly

24   different EC connections between patients and controls. UWS patients show connections with both

25   decreased and increased EC (decreased in fronto-temporal, frontal-parietal and midline regions;

26   increased in subcortical and wide cortical areas). MCS patients show decreased EC in fronto-

27   temporal and interhemispheric midline connections. Blue and red arrows indicate lower and higher

25

1   EC respectively in patients as compared to HC subjects. The directional connections in the glass

2   brain represents connections with significant between-group differences (Bonferroni corrected for

3   11395 tests, p-value < 0.05) are represented.

4   **Figure 3. *In-silico* propagation of exogenous perturbations.** (a) Temporal evolution of the

5   response matrices R(t) for healthy controls (HC) and patients (unresponsive wakefulness

6   syndrome, UWS; minimally conscious state, MCS) at different times (early = 2 sec, middle = 20

7   sec, late 60 sec and very late = 200 sec). Matrix elements $R_{ij}(t)$ represent the conditional response

8   at region j due to a unit perturbation applied at region i at time t = 0. Note that here time corresponds

9   to the arbitrary simulation time after the *in-silico* perturbation is applied and thus it does not

10 correspond to actual time, although the time-constants governing the evolution were estimated

11 from the BOLD signals. The colorbar represents the relative strength of the response between brain

12 regions (unitless). (b) Whole brain response curves for the three study cases reflecting the sum of

13 all pair-wise responses at each time point post-stimulus. Shaded areas represent the 95%

14 confidence intervals across subjects. Black stars indicate a difference in global responses between

15 all three groups (Bonferroni corrected for 100 tests/time points, p-value=0.05). Red stars indicate

16 the early epoch during which UWS patients display a larger response than HC and MCS

17 (Bonferroni corrected for 100 tests/time points, p-value=0.05). Inset: Area-under-the-curve for the

18 three global response curves in the time range t = 60 – 200 sec, quantifying the differences across

19 the three groups.

20 **Figure 4. Region-wise broadcasting and receiving capacities due to exogenous perturbations.**

21 Maps of significantly large broadcasting and receiving capacities for the three study groups

22 (healthy controls, HC; unresponsive wakefulness syndrome, UWS; and minimally conscious state,

23 MCS). The color code represents the t-values. Only regions with significantly high values are

24 presented in each case (FDR corrected p-values <0.05 for 214 tests (ROIs)).

25 **Figure 5. Group comparison of regional broadcasting and receiving capacities after**

26 **exogenous perturbations.** Maps of regional contrasts in broadcasting and receiving capacity

27 between study groups. Color bar represents the t-values for regions with significant between-group

28 differences (Bonferroni corrected p-values <0.05 for 214 tests (ROIs)).

26

1   **Supplementary Figure 1.** Spatial maps showing the regional distribution of relaxation time

2   constants (τ) as calculated for empirical BOLD signals for each area. Healthy controls display a

3   spatial heterogeneous distribution of τ, while UWS patients are characterized by short time

4   constants overall. The spatial distribution of regional τ is very much recovered in MCS patients.

5   **Supplementary Figure 2.** Brain regions' hyper-response (higher growth with sudden decay) differ

6   in (a) UWS patients compared to HC (b) MCS patients compared to HC (c) UWS compared to

7   MCS patients for receiving and broadcasting capacities. Color bar represents the t-values for

8   regions with significant between-group differences (Bonferroni corrected for 214 tests).

27
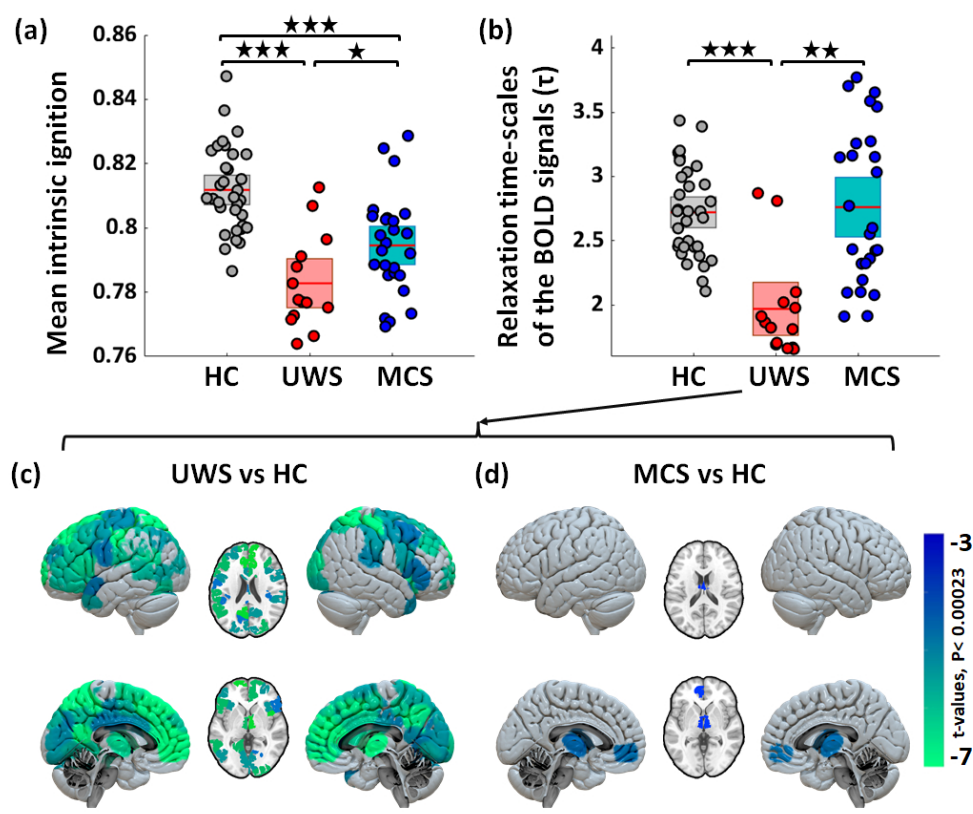
Figure 1. Changes in endogenous properties from resting-state BOLD signals. Healthy controls (HC), unresponsive wakefulness syndrome (UWS) and minimally conscious state (MCS) (a) Comparison of mean intrinsic ignition for the three groups, illustrating the reduced capacity to integrate endogenous spontaneous events in patients with DOC. (b) Relaxation time-scales of the BOLD signals (τ) at the whole-brain level shows significant reductions in UWS and MCS patients compared to HC. Stars reflect the Bonferroni corrected (for three groups) significance levels (*=p-value<0.016; **= p-value<0.001; ***= p-value<0.0001). (c,d) Maps of significant differences in regional distributions of τ between patients and controls. The color bar represents the t-values of significant between-group differences (Bonferroni corrected for 214 tests, p-value=0.05).

369x312mm (72 x 72 DPI)
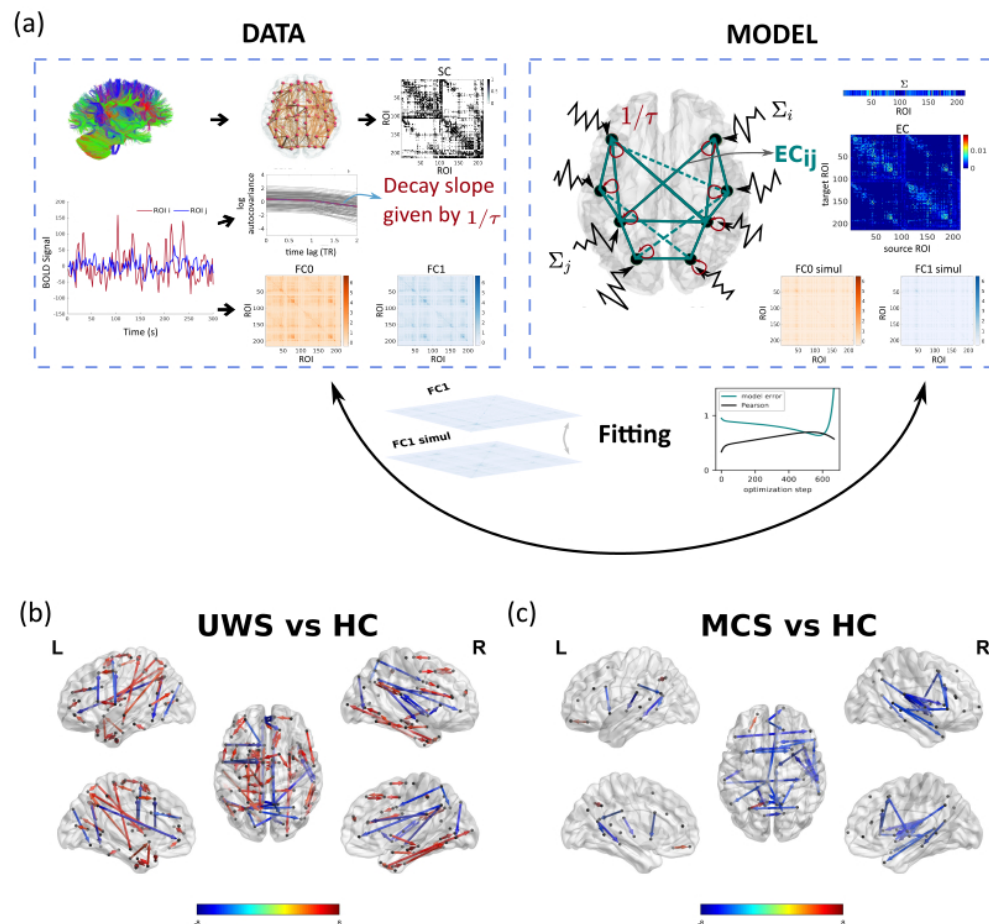
Figure 2. Comparison of effective connectivity (EC) between healthy controls and patients. (a) Schematic representation of the fitting procedure leading to estimation of EC. Considering a model of noise diffusion – the multivariate Ornstein-Uhlenbeck process – the whole-brain network model is constrained using structural connectivity obtained from diffusion imaging and then fitted to reproduce the empirical resting-state data. In particular, to fit the zero-lag and 1TR-lag covariance matrices (FC0 and FC1), and the regional noise level Σi. (b, c) Maps of significantly different EC connections between patients and controls. UWS patients show connections with both decreased and increased EC (decreased in fronto-temporal, frontal-parietal and midline regions; increased in subcortical and wide cortical areas). MCS patients show decreased EC in fronto-temporal and interhemispheric midline connections. Blue and red arrows indicate lower and higher EC respectively in patients as compared to HC subjects. The directional connections in the glass brain represents connections with significant between-group differences (Bonferroni corrected for 11395 tests, p-value < 0.05) are represented.

540x513mm (38 x 38 DPI)
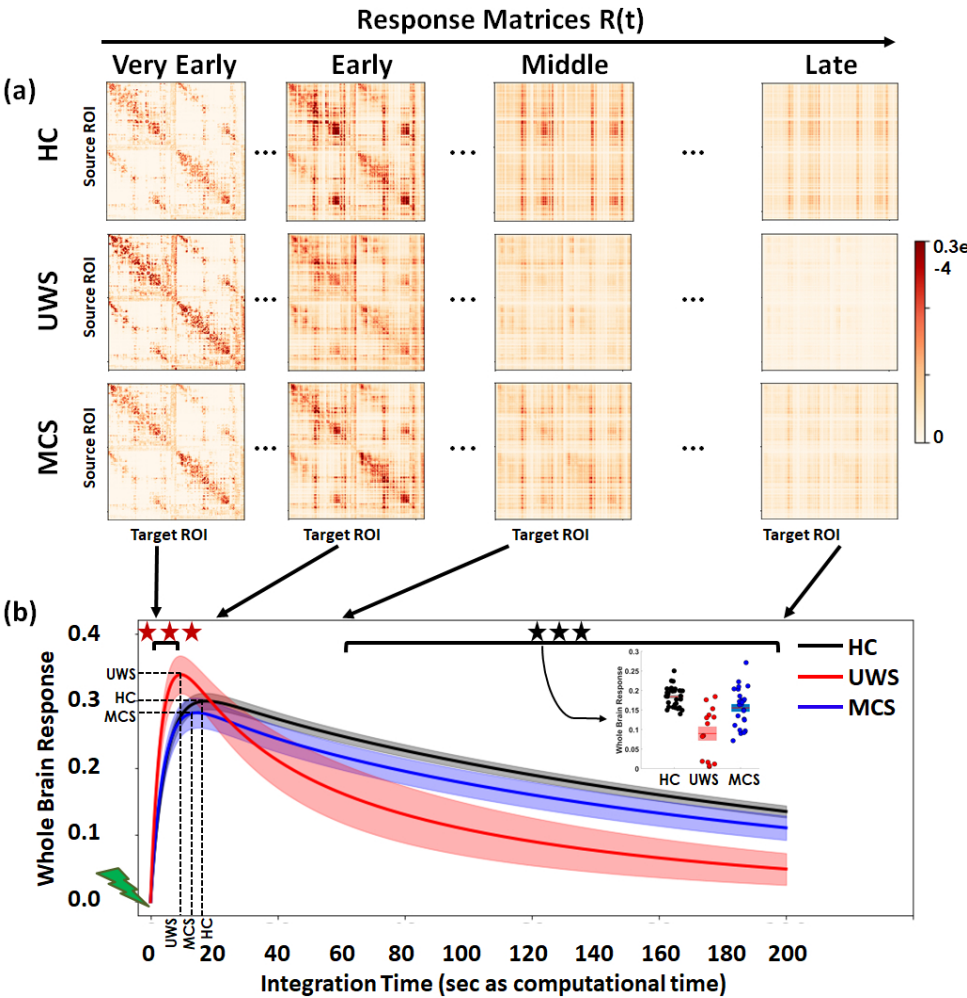
Figure 3. In-silico propagation of exogenous perturbations. (a) Temporal evolution of the response matrices R(t) for healthy controls (HC) and patients (unresponsive wakefulness syndrome, UWS; minimally conscious state, MCS) at different times (early = 2 sec, middle = 20 sec, late 60 sec and very late = 200 sec). Matrix elements Rij(t) represent the conditional response at region j due to a unit perturbation applied at region i at time t = 0. Note that here time corresponds to the arbitrary simulation time after the in-silico perturbation is applied and thus it does not correspond to actual time, although the time-constants governing the evolution were estimated from the BOLD signals. The colorbar represents the relative strength of the response between brain regions (unitless). (b) Whole brain response curves for the three study cases reflecting the sum of all pair-wise responses at each time point post-stimulus. Shaded areas represent the 95% confidence intervals across subjects. Black stars indicate a difference in global responses between all three groups (Bonferroni corrected for 100 tests/time points, p-value=0.05). Red stars indicate the early epoch during which UWS patients display a larger response than HC and MCS (Bonferroni corrected for 100 tests/time points, p-value=0.05). Inset: Area-under-the-curve for the three global response curves in the time range t = 60 – 200 sec, quantifying the differences across the three groups.

375x382mm (72 x 72 DPI)
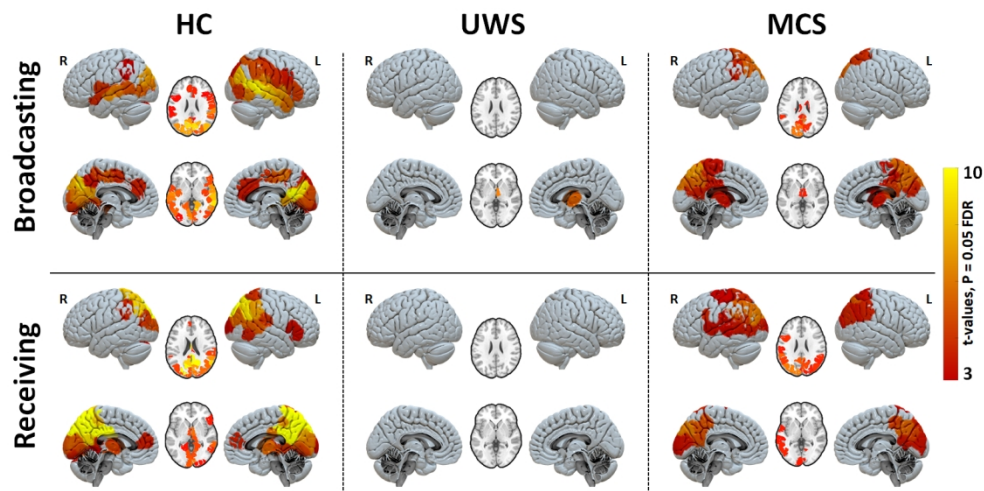
Figure 4. Region-wise broadcasting and receiving capacities due to exogenous perturbations. Maps of significantly large broadcasting and receiving capacities for the three study groups (healthy controls, HC; unresponsive wakefulness syndrome, UWS; and minimally conscious state, MCS). The color code represents the t-values. Only regions with significantly high values are presented in each case (FDR corrected p-values <0.05 for 214 tests (ROIs)).

579x305mm (72 x 72 DPI)
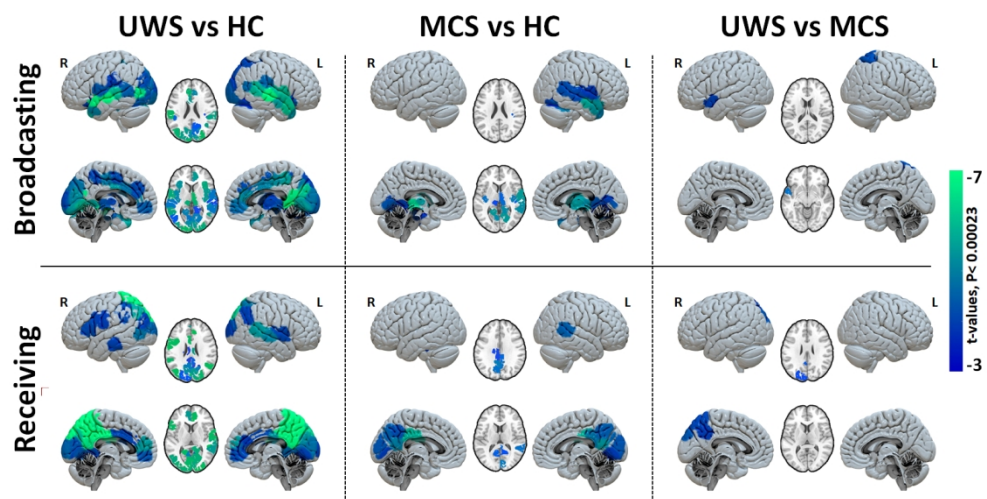
Figure 5. Group comparison of regional broadcasting and receiving capacities after exogenous perturbations. Maps of regional contrasts in broadcasting and receiving capacity between study groups. Color bar represents the t-values for regions with significant between-group differences (Bonferroni corrected p-values <0.05 for 214 tests (ROIs)).

576x305mm (72 x 72 DPI)

Posterior integration and thalamo-frontotemporal broadcasting are impaired in disorders of consciousness

Rajanikant Panda[1,2*,§], Ane López-González[3*,§], Matthieu Gilson[3,4], Olivia Gosseries[1,2], Aurore Thibaut[1,2], Gianluca Frasso[5], Benedetta Cecconi[1,2], Anira Escrichs[3], Gustavo Deco[3,6,7,8], Steven Laureys[1,2,9], Gorka Zamora-López[3#], Jitka Annen[1,2#]

*These Author Contributed Equally

#These authors share supervision

MRI Data Analysis:

Functional MRI data preprocessing

Preprocessing was performed using MELODIC (Multivariate Exploratory Linear Optimized Decomposition into Independent Components) version 3.14, which is part of FMRIB's Software Library (FSL, http://fsl.fmrib.ox.ac.uk/fsl). The preprocessing consisted of the following steps: the first five functional images were discarded to reduce scanner inhomogeneity, motion correction was performed using MCFLIRT, non-brain tissue was removed using BET, intensity was normalized, temporal band-pass filtering with sigma 100 sec was performed, spatial smoothing was applied using a 5mm FWHM Gaussian kernel, rigid-body registration and single-session ICA with automatic dimensionality. Then noise components and lesion-driven artifacts (e.g., head movement, metal, and physiological noise artifacts) were manually regressed out for each subject. Specifically, FSLeyes in Melodic mode was used to identify the single-subject Independent Components (ICs) into "good" for cerebral signal, "bad" for noise or injury-driven artifacts, and "unknown" for ambiguous components. Each component was evaluated based on the spatial map, the time series, and the temporal power spectrum.[1] FIX was applied with default parameters to remove bad and lesion-driven artifacts components.[1] Subsequently, the Shen et al (2015) functional resting state atlas (without cerebellum) was used for parcellation to obtain the BOLD time series of the 214 cortical and subcortical brain areas in each individual's native EPI space.[2] The cleaned functional data were co-registered to the T1-weighted structural image using FLIRT. Then, the T1-weighted image was co-registered to the standard MNI space by using FLIRT (12 DOF), and FNIRT.[3] This transformation matrix was inverted and applied to warp the resting-state atlas from MNI space to the single-subject functional data. Finally, the time series for each of the 214 brain areas were extracted using custom-made Matlab scripts using 'fslmaths' and 'fslmeants'.

1

1   **Structural Connectivity Matrix**

2   We computed an average whole-brain structural connectivity matrix from all healthy participants
3   as described in our previous study.[4] Briefly, the b0 image in native diffusion space was co-
4   registered to the T1 structural image using FLIRT.[3] Next, the T1 structural image was co-register
5   to the MNI space by using FLIRT and FNIRT.[3] The resulting transformations were inverted and
6   applied to warp the resting-state atlas from MNI space to the native diffusion space using a nearest-
7   neighbor interpolation method. Then, analysis of diffusion images was performed using the
8   FMRIB's Diffusion Toolbox (FDT) www.fmrib.ox.ac.uk/fsl. Brain Extraction Tool was
9   computed, and eddy current distortions and head motion were corrected using eddy correct tool [5].
10   Furthermore, the gradient matrix was reoriented to correct for the subject. Then, Crossing Fibres
11   were modeled using the default BEDPOSTX parameters, and the probability of multi-fibre
12   orientations was calculated to improve the sensitivity of non-dominant fibre populations [5]. Next,
13   probabilistic tractography was calculated in native diffusion space using the default PROB-
14   TRACKX settings[5] to estimate the connectivity probability of each brain area to each of the other
15   213 brain areas. Subsequently, to obtain the structural probability matrix, the value of each brain
16   area was divided by its corresponding number of generated tracts. Given that probabilistic
17   tractography does not capture fiber directionality, the SCnp matrix was symmetrized by computing
18   their transpose matrix SCpn and averaging both matrices. Finally a group structural connectivity
19   (SC) mask was obtained by averaging the all HC subjects' SC matrix and applying a threshold of
20   80% to maintain the top 20% of strongest connections to binarize the SC. This SC mask was used
21   to constrain the functional connectivity matrix for the whole brain EC computation.

22   **Phase-locking matrices**

23   The instantaneous level of pairwise synchronization was calculated by the phase-locking value
24   between two brain regions. First, the BOLD signals were filtered within a narrowband of 0.01-
25   0.09 Hz. Then the instantaneous phases $\varphi_k(t)$ were computed using the Hilbert transform for each
26   BOLD signal individually. This yields the associated analytical signal which represents a
27   narrowband signal s(t) in the time domain as a rotating vector with an instantaneous phase
28   $\phi(t)$ and an instantaneous amplitude, A(t). That is, s(t) = A(t)cos(φ(t)). Given the instantaneous
29   phases $\phi_j(t)$ and $\phi_k(t)$ calculated two brain regions from their corresponding BOLD signals, the
30   pairwise synchronization $P_{jk}(t)$ was defined as the cosine similarity of the two phases:

31   $$P_{jk}(t) = \cos\left(|\phi_j(t) - \phi_k(t)|\right)$$

32   Thus, $P_{jk}(t) = 1$ when the two regions are in phase, $P_{jk}(t) = 0$ when they are orthogonal and P_{jk}
33   (t) = -1 when they are in anti-phase.

34

2

References

1. Griffanti L, Douaud G, Bijsterbosch J, et al. Hand classification of fMRI ICA noise components. *Neuroimage*. 2017;154.
2. Finn ES, Shen X, Scheinost D, et al. Functional connectome fingerprinting: Identifying individuals based on patterns of brain connectivity HHS Public Access Author manuscript. *Nat Neurosci*. 2015;18(11).
3. Smith SM, Jenkinson M, Woolrich MW, et al. Advances in functional and structural MR image analysis and implementation as FSL. In: *NeuroImage*. Vol 23. ; 2004.
4. López-González A, Panda R, Ponce-Alvarez A, et al. Loss of consciousness reduces the stability of brain hubs and the heterogeneity of brain dynamics. *bioRxiv*. Published online November 22, 2020:2020.11.20.391482.
5. Behrens TEJ, Woolrich MW, Jenkinson M, et al. Characterization and Propagation of Uncertainty in Diffusion-Weighted MR Imaging. *Magn Reson Med*. 2003;50(5).

Supplementary Figures:
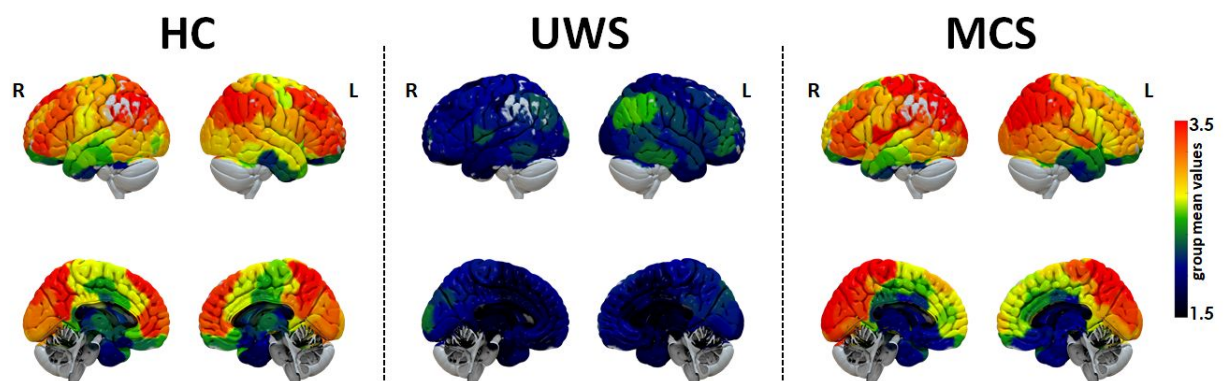
Supplementary Figure 1. Spatial maps showing the regional distribution of relaxation time constants (τ) as calculated for empirical BOLD signals for each area. Healthy controls display a spatial heterogeneous distribution of τ, while UWS patients are characterized by short time constants overall. The spatial distribution of regional τ is very much recovered in MCS patients.

3
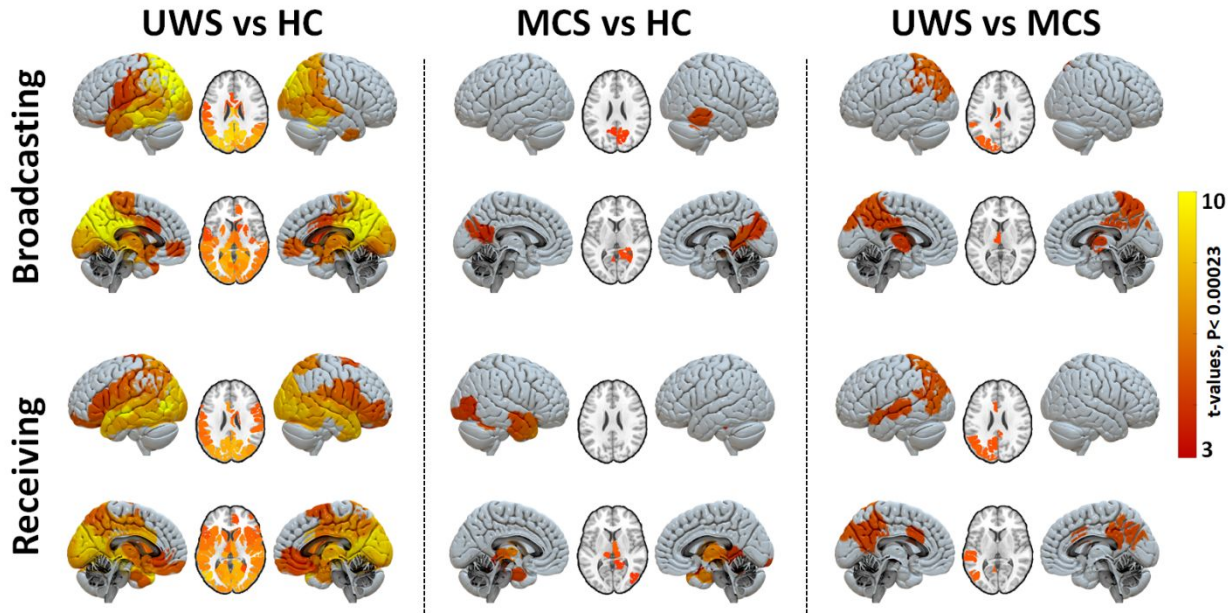
Supplementary Figure 2. Brain regions' hyper-response (higher growth with sudden decay) differ in (a) UWS patients compared to HC (b) MCS patients compared to HC (c) UWS compared to MCS patients for receiving and broadcasting capacities. Color bar represents the t-values for regions with significant between-group differences (Bonferroni corrected for 214 tests).

1

2

3

4

5

6

7

8

9

10

11

12

13

14

15

16

17

4

Supplementary Table

Supplementary Table S1. MCS and UWS patients' demographic and clinical characteristics.

The table includes condition, etiology (traumatic brain injury (TBI) and cerebral vascular accident (CVA)), time science injury (TSI), age, gender (F=female, M=male), Coma Recovery Scale-Revised (CSR-R) auditory, visual, motor, verbal, communication and arousal subscores, total and CSR-R Index.

Patient ID	Etiology	TSI (Days)	Age (Years)	Gender	Auditory	Visual	Motor	Verbal	Communication	Arousal	Total CSRR	CSRR Index
MCS P1	TBI	3034	34	F	3	3	2	2	0	2	12	33.0
MCS P2	TBI	1294	40	F	2	3	2	2	0	2	11	24.6
MCS P3	CAV	13	62	M	0	3	2	1	0	1	7	21.2
MCS P4	Haemorrhage Stroke	389	59	F	2	1	2	1	0	2	8	22.5
MCS P5	TBI	589	30	M	3	2	2	2	0	1	10	24.3
MCS P6	TBI	521	28	M	1	3	2	2	0	2	10	23.6
MCS P7	TBI	533	47	M	3	5	2	1	0	2	13	48.6
MCS P8	CVA	2639	38	M	1	3	2	2	0	1	9	23.3
MCS P9	TBI	2690	24	M	3	3	5	1	0	2	14	48.6
MCS P10	Anoxia	9900	39	M	3	3	5	2	0	2	15	49.6
MCS P11	TBI & Anoxia	314	26	F	3	1	2	1	0	2	9	15.3
MCS P12	TBI	407	31	M	0	1	5	2	0	1	9	15.5
MCS P13	Anoxia	64	29	M	1	3	2	2	0	2	10	23.6
MCS P14	Anoxia	639	43	M	2	3	1	2	0	2	10	23.6
MCS P15	TBI	1241	53	M	0	3	2	2	0	2	9	22.5
MCS P16	TBI	135	51	M	3	4	2	1	0	2	12	40.3
MCS P17	Haemorrhage Stroke	1383	68	F	3	1	3	2	0	2	11	16.3
MCS P18	TBI	1331	35	M	3	0	2	1	0	2	8	14.2
MCS P19	TBI – Haemorrhage Stroke	35	73	M	0	2	0	1	0	1	4	10.8
MCS P20	CVA	104	43	F	3	1	3	1	0	0	8	14.6

5

MCS P21	TBI & Anoxia	401	29	M	1	3	2	1	0	2	9	22.5
MCS P22	TBI – Haemorrhage Stroke	255	39	M	4	5	4	2	1	2	18	66.3
MCS P23	Anoxia	1482	32	M	3	4	2	2	1	2	14	41.3
MCS P24	TBI	641	23	M	3	3	0	1	0	2	9	29.8
MCS P25	CVA	34	47	F	3	4	5	3	2	2	19	66.3
MCS P26	Anoxia	7814	34	M	1	3	5	2	0	2	13	48.6
UWS P1	TBI	283	52	F	1	0	2	2	0	1	6	5.5
UWS P2	Anoxia	743	30	M	1	0	2	1	0	2	6	4.8
UWS P3	Anoxia	92	74	M	1	0	1	1	0	1	4	3.5
UWS P4	Haemorrhage Stroke	43	64	M	1	0	2	1	0	1	5	4.5
UWS P5	Anoxia	18	20	M	1	0	0	1	0	1	3	2.4
UWS P6	Anoxic Asphyxia	304	60	F	1	1	1	1	0	2	6	4.8
UWS P7	Anoxia	29	44	M	1	0	1	0	0	2	4	2.7
UWS P8	Anoxia	38	50	F	0	0	0	2	0	1	3	2.4
UWS P9	Anoxia	50	69	F	0	1	2	1	0	1	5	4.5
UWS P10	Anoxia	1868	21	F	1	0	1	2	0	2	6	4.8
UWS P11	Anoxia	129	49	F	1	0	0	1	0	2	4	2.7
UWS P12	TBI	24	58	M	0	1	2	0	0	1	4	4.2
UWS P13	Anoxia	30	44	M	1	1	1	1	0	1	5	4.5
UWS P14	Anoxia	335	40	F	1	0	2	1	0	2	6	4.8

1
2
3
4
5
6
7
8
9

1 **Supplementary Table 2.** Regional difference in local Relaxation time-scales of the BOLD
2 signals (τ) for UWS patients vs HC and MCS patients vs HC (Bonferroni Corrected).
3

No	Brain Region with different τ for UWS vs HC	t-value	p-value
1	44% Frontal_Med_VMPFC_R / 31% Cingulum_Ant_R	-5.1	5.62E-06
2	34% Frontal_Sup_R / 33% Frontal_Sup_Medial_R	-5.2	4.21E-06
3	41% Frontal_Mid_Orb_R / 29% Frontal_Mid_R	-4.9	1.37E-05
4	60% Frontal_Sup_Medial_R / 20% Cingulum_Ant_R	-6.0	2.83E-07
5	84% Frontal_Mid_R	-5.1	5.72E-06
6	52% Frontal_Sup_R / 41% Frontal_Sup_Medial_R	-5.0	1.05E-05
7	51% Frontal_Mid_R / 38% Frontal_Sup_R	-5.9	4.35E-07
8	85% Frontal_Mid_R	-3.9	0.0002
9	56% Cingulum_Mid_R / 26% Cingulum_Ant_R	-5.2	5.50E-06
10	45% Frontal_Inf_Tri_R / 28% Frontal_Inf_Orb_R	-3.9	0.0002
11	57% Insula_R / 21% Frontal_Inf_Tri_R	-4.5	5.41E-05
12	45% Frontal_Inf_Oper_R / 34% Precentral_R	-4.6	3.91E-05
13	44% Frontal_Inf_Oper_R / 34% Frontal_Inf_Tri_R	-4.2	0.0001
14	74% Supp_Motor_Area_R	-5.2	4.28E-06
15	51% Precentral_R / 43% Frontal_Sup_R	-4.5	4.09E-05
16	81% Precentral_R	-4.4	7.53E-05
17	60% Supp_Motor_Area_R / 22% Cingulum_Mid_R	-5.7	8.54E-07
18	58% Supp_Motor_Area_R / 42% Frontal_Sup_R	-4.6	4.00E-05
19	47% Frontal_Mid_R / 40% Frontal_Sup_R	-5.6	1.09E-06
20	45% Precentral_R / 25% Frontal_Mid_R	-5.1	6.44E-06
21	66% Postcentral_R	-6.7	3.12E-08
22	66% Insula_R	-6.3	1.30E-07
23	52% Insula_R / 36% Frontal_Inf_Orb_R	-5.3	3.75E-06
24	47% Postcentral_R / 23% Parietal_Inf_R	-4.8	1.60E-05
25	70% Parietal_Sup_R	-6.4	7.25E-08
26	37% Parietal_Sup_R / 23% Parietal_Inf_R	-5.1	6.70E-06
27	80% Precuneus_R	-4.7	2.46E-05
28	47% SupraMarginal_R / 35% Postcentral_R	-4.5	4.47E-05
29	53% Temporal_Sup_R / 37% SupraMarginal_R	-4.2	0.0001
30	62% Temporal_Pole_Mid_R	-4.2	0.0001
31	28% Temporal_Sup_R / 25% Rolandic_Oper_R	-4.1	0.0002
32	51% Lingual_R / 33% Fusiform_R	-3.9	0.0002
33	67% Occipital_Mid_R	-5.5	1.48E-06
34	42% Occipital_Sup_R / 26% Cuneus_R	-4.6	3.08E-05
35	48% Lingual_R / 17% Fusiform_R	-4.3	8.05E-05
36	37% Occipital_Mid_R / 20% Occipital_Sup_R	-5.2	4.03E-06
37	78% Lingual_R	-4.7	2.53E-05

7

38	39% Calcarine_R / 27% Cuneus_R	-4.5	5.39E-05
39	59% Occipital_Inf_R / 23% Lingual_R	-4.8	1.91E-05
40	76% Calcarine_R	-4.0	0.0002
41	81% Cingulum_Ant_R	-5.9	3.94E-07
42	81% Cingulum_Mid_R	-5.3	3.84E-06
43	57% Precuneus_R / 32% Calcarine_R	-4.3	0.0001
44	42% Cingulum_Mid_R	-4.5	5.11E-05
45	79% Precuneus_R	-5.8	6.66E-07
46	46% Precuneus_R / 37% Cingulum_Mid_R	-5.2	5.48E-06
47	62% Caudate_R	-5.2	4.15E-06
48	52% Thalamus_R	-6.3	1.12E-07
49	54% Frontal_Med_VMPFC_L / 31% Cingulum_Ant_L	-7.8	7.11E-10
50	50% Frontal_Sup_Medial_L / 47% Cingulum_Ant_L	-8.0	4.01E-10
51	40% Frontal_Sup_Medial_L / 30% Frontal_Sup_L	-6.0	3.48E-07
52	40% Frontal_Mid_Orb_L / 39% Frontal_Inf_Orb_L	-4.9	1.39E-05
53	75% Frontal_Mid_L	-4.4	7.13E-05
54	57% Frontal_Sup_Medial_L / 41% Frontal_Sup_L	-5.1	6.47E-06
55	66% Frontal_Mid_L	-6.0	3.34E-07
56	63% Frontal_Inf_Tri_L	-5.1	6.24E-06
57	44% Frontal_Sup_Medial_L / 43% Frontal_Sup_L	-6.4	8.02E-08
58	84% Frontal_Mid_L	-4.9	1.35E-05
59	55% Supp_Motor_Area_L / 24% Frontal_Sup_Medial_L	-5.9	4.70E-07
60	64% Frontal_Inf_Orb_L	-5.0	8.11E-06
61	61% Frontal_Inf_Tri_L	-5.0	9.00E-06
62	66% Insula_L	-4.4	5.78E-05
63	52% Frontal_Inf_Tri_L / 42% Frontal_Inf_Oper_L	-5.3	3.05E-06
64	50% Precentral_L / 30% Frontal_Inf_Oper_L	-4.3	9.68E-05
65	63% Postcentral_L	-5.8	6.24E-07
66	68% Postcentral_L	-4.1	0.0002
67	52% Cingulum_Mid_L / 45% Supp_Motor_Area_L	-4.8	1.52E-05
68	81% Supp_Motor_Area_L	-5.4	2.07E-06
69	46% Frontal_Mid_L / 45% Frontal_Sup_L	-6.0	2.95E-07
70	81% Precentral_L	-4.5	5.22E-05
71	57% Precentral_L / 22% Frontal_Sup_L	-5.0	8.45E-06
72	51% Postcentral_L / 39% Precentral_L	-4.3	0.0001
73	54% Postcentral_L / 28% Parietal_Inf_L	-6.6	3.81E-08
74	61% Postcentral_L	-4.0	0.0002
75	66% Parietal_Sup_L	-6.6	3.65E-08
76	45% Cuneus_L / 40% Precuneus_L	-4.1	0.0002

8

77	31% Parietal_Inf_L / 24% Parietal_Sup_L	-6.0	3.46E-07
78	75% Precuneus_L	-6.0	2.98E-07
79	49% Parietal_Inf_L / 38% Postcentral_L	-6.2	1.56E-07
80	44% Temporal_Sup_L / 26% Rolandic_Oper_L	-4.1	0.0002
81	40% SupraMarginal_L / 32% Temporal_Sup_L	-5.2	5.44E-06
82	59% Angular_L / 26% Parietal_Inf_L	-4.5	5.35E-05
83	55% Temporal_Mid_L / 27% Angular_L	-5.3	3.02E-06
84	57% Parietal_Inf_L / 36% SupraMarginal_L	-4.9	1.11E-05
85	57% Temporal_Pole_Mid_L / 25% Temporal_Mid_L	-4.6	3.69E-05
86	54% Temporal_Pole_Sup_L / 27% Temporal_Sup_L	-4.1	0.0002
87	82% Temporal_Mid_L	-4.9	1.23E-05
88	71% Fusiform_L	-4.7	2.64E-05
89	93% Occipital_Mid_L	-4.7	2.88E-05
90	57% Lingual_L / 21% Calcarine_L	-5.0	9.29E-06
91	49% Occipital_Inf_L / 33% Fusiform_L	-5.1	6.21E-06
92	47% Occipital_Sup_L / 32% Cuneus_L	-4.9	1.30E-05
93	41% Temporal_Mid_L / 35% Occipital_Mid_L	-4.7	2.89E-05
94	88% Lingual_L	-4.8	1.87E-05
95	38% Lingual_L / 20% Calcarine_L	-4.5	5.15E-05
96	67% Calcarine_L	-4.3	9.30E-05
97	66% Cingulum_Mid_L	-4.3	9.92E-05
98	50% Cingulum_Ant_L / 39% Frontal_Sup_Medial_L	-5.7	7.71E-07
99	62% Cingulum_Mid_L	-4.1	0.0002
100	37% Cingulum_Mid_L / 36% Cingulum_Ant_L	-4.4	7.67E-05
101	45% Precuneus_L / 34% Calcarine_L	-5.9	4.04E-07
102	39% Cingulum_Mid_L / 22% Cingulum_Post_L	-4.0	0.0002
103	74% Precuneus_L	-5.0	8.90E-06
104	46% Precuneus_L / 45% Cingulum_Mid_L	-5.9	4.78E-07
105	43% ParaHippocampal_L / 24% Hippocampus_L	-5.1	5.73E-06
106	53% Thalamus_L	-5.3	3.17E-06
No	**Brain Region with different τ for MCS vs HC**	**t-value**	**p-value**
1	52% Thalamus_R	4.1	0.0002
2	53% Thalamus_L	4.0	0.0002
3	54% Frontal_Med_VMPFC_L / 31% Cingulum_Ant_L	4.1	0.0002

9

1 **Supplementary Table 3:** Brain Regions have significantly large broadcasting and receiving
2 capacities for the three study groups (healthy controls, HC; unresponsive wakefulness syndrome,
3 UWS; and minimally conscious state, MCS). The regions with significantly high values are
4 presented in each case (FDR corrected p-values <0.05 for 214 tests (ROIs)).
5

NO	HC Broadcasting Capacities	p-value	t-value
1	56% Cingulum_Mid_R / 26% Cingulum_Ant_R	0.0015	3.2
2	45% Frontal_Inf_Tri_R / 28% Frontal_Inf_Orb_R	8.75E-05	4.2
3	45% Frontal_Inf_Oper_R / 34% Precentral_R	0.0022	3.1
4	44% Frontal_Inf_Oper_R / 34% Frontal_Inf_Tri_R	0.0163	2.2
5	74% Postcentral_R	0.0003	3.7
6	66% Insula_R	0.0001	4.0
7	34% Insula_R / 22% Putamen_R	0.0002	3.8
8	47% Postcentral_R / 23% Parietal_Inf_R	0.0016	3.2
9	57% Rolandic_Oper_R / 34% Insula_R	0.0003	3.7
10	49% Precuneus_R / 40% Cuneus_R	5.74E-09	7.6
11	37% Parietal_Sup_R / 23% Parietal_Inf_R	1.38E-05	4.9
12	47% SupraMarginal_R / 35% Postcentral_R	0.0002	3.9
13	53% Temporal_Sup_R / 37% SupraMarginal_R	3.56E-07	6.1
14	46% SupraMarginal_R / 34% Parietal_Inf_R	3.10E-05	4.6
15	73% Occipital_Mid_R	3.46E-09	7.8
16	87% Temporal_Mid_R	1.49E-10	9.0
17	45% Temporal_Pole_Sup_R / 34% Temporal_Pole_Mid_R	1.68E-06	5.6
18	58% Temporal_Mid_R / 32% Temporal_Sup_R	6.61E-05	4.3
19	50% Temporal_Sup_R / 28% Rolandic_Oper_R	6.67E-08	6.7
20	28% Temporal_Sup_R / 25% Rolandic_Oper_R	2.52E-08	7.1
21	52% Temporal_Sup_R / 48% Temporal_Mid_R	1.52E-09	8.1
22	66% Temporal_Mid_R	2.28E-08	7.1
23	64% Temporal_Mid_R	7.79E-11	9.2
24	53% Fusiform_R / 16% Lingual_R	0.0113	2.4
25	51% Temporal_Inf_R / 47% Temporal_Mid_R	4.67E-07	6.1
26	51% Lingual_R / 33% Fusiform_R	0.0001	4.0
27	67% Occipital_Mid_R	3.79E-06	5.3
28	34% Occipital_Mid_R / 32% Temporal_Mid_R	0.0002	3.9
29	42% Occipital_Sup_R / 26% Cuneus_R	3.44E-03	2.9
30	48% Lingual_R / 17% Fusiform_R	0.0015	3.2
31	65% Cuneus_R	1.23E-10	9.1
32	78% Lingual_R	4.34E-05	4.5
33	39% Calcarine_R / 27% Cuneus_R	4.07E-05	4.5
34	76% Calcarine_R	6.00E-11	9.3
35	81% Cingulum_Ant_R	0.0021	3.1

10

36	57% Precuneus_R / 32% Calcarine_R	4.44E-15	13.5
37	80% Cingulum_Mid_R	1.59E-05	4.8
38	79% Precuneus_R	1.11E-02	2.4
39	46% Precuneus_R / 37% Cingulum_Mid_R	1.17E-06	5.7
40	49% Lingual_R / 23% Precuneus_R	1.06E-08	7.4
41	50% Precentral_L / 30% Frontal_Inf_Oper_L	0.0118	2.4
42	52% Cingulum_Mid_L / 45% Supp_Motor_Area_L	0.0004	3.6
43	37% Temporal_Sup_L / 35% Rolandic_Oper_L	0.0001	4.0
44	34% Insula_L / 18% Temporal_Sup_L	1.43E-05	4.9
45	45% Cuneus_L / 40% Precuneus_L	1.65E-10	8.9
46	31% Parietal_Inf_L / 24% Parietal_Sup_L	3.60E-06	5.3
47	44% Temporal_Sup_L / 26% Rolandic_Oper_L	0.0001	4.0
48	40% SupraMarginal_L / 32% Temporal_Sup_L	0.0131	2.3
49	57% Parietal_Inf_L / 36% SupraMarginal_L	0.0082	2.5
50	54% Temporal_Pole_Sup_L / 27% Temporal_Sup_L	0.0004	3.7
51	62% Temporal_Mid_L	1.28E-06	5.7
52	82% Temporal_Mid_L	2.57E-05	4.7
53	72% Temporal_Mid_L	2.26E-07	6.3
54	73% Occipital_Mid_L	9.28E-08	6.6
55	93% Occipital_Mid_L	8.77E-07	5.8
56	57% Lingual_L / 21% Calcarine_L	1.69E-05	4.8
57	40% Fusiform_L / 31% Lingual_L	0.0121	2.4
58	47% Occipital_Sup_L / 32% Cuneus_L	1.69E-08	7.2
59	41% Temporal_Mid_L / 35% Occipital_Mid_L	6.69E-06	5.1
60	49% Occipital_Mid_L / 44% Occipital_Inf_L	0.0105	2.4
61	88% Lingual_L	5.62E-07	6.0
62	38% Lingual_L / 20% Calcarine_L	0.0004	3.7
63	67% Calcarine_L	7.85E-08	6.7
64	66% Cingulum_Mid_L	1.33E-05	4.9
65	50% Cingulum_Ant_L / 39% Frontal_Sup_Medial_L	0.0008	3.4
66	45% Precuneus_L / 34% Calcarine_L	4.78E-08	6.8
67	74% Precuneus_L	3.35E-03	2.9
68	46% Precuneus_L / 45% Cingulum_Mid_L	9.70E-05	4.2
69	43% ParaHippocampal_L / 24% Hippocampus_L	3.45E-05	4.6
No	**MCS Broadcasting Capacities**	**p-value**	**t-value**
1	70% Parietal_Sup_R	0.0043	2.9
2	49% Precuneus_R / 40% Cuneus_R	0.0002	4.1
3	37% Parietal_Sup_R / 23% Parietal_Inf_R	2.30E-05	4.9
4	46% SupraMarginal_R / 34% Parietal_Inf_R	0.0011	3.4

11

5	87% Angular_R	0.0033	3.0
6	73% Occipital_Mid_R	0.0007	3.6
7	67% Occipital_Mid_R	0.0030	3.0
8	42% Occipital_Sup_R / 26% Cuneus_R	1.30E-03	3.3
9	65% Cuneus_R	0.0001	4.3
10	39% Calcarine_R / 27% Cuneus_R	0.0034	3.0
11	76% Calcarine_R	0.0026	3.1
12	57% Precuneus_R / 32% Calcarine_R	0.0026	3.1
13	79% Precuneus_R	1.01E-05	5.2
14	46% Precuneus_R / 37% Cingulum_Mid_R	0.0002	4.2
15	50% Precentral_L / 30% Frontal_Inf_Oper_L	0.0008	3.5
16	37% Temporal_Sup_L / 35% Rolandic_Oper_L	0.0044	2.8
17	51% Postcentral_L / 39% Precentral_L	0.0078	2.6
18	66% Parietal_Sup_L	6.72E-04	3.6
19	45% Cuneus_L / 40% Precuneus_L	9.45E-07	6.2
20	31% Parietal_Inf_L / 24% Parietal_Sup_L	3.90E-06	5.6
21	40% SupraMarginal_L / 32% Temporal_Sup_L	0.0041	2.9
22	59% Angular_L / 26% Parietal_Inf_L	5.45E-06	5.5
23	55% Temporal_Mid_L / 27% Angular_L	0.0003	3.9
24	57% Parietal_Inf_L / 36% SupraMarginal_L	1.64E-05	5.0
25	62% Temporal_Mid_L	0.0067	2.7
26	82% Temporal_Mid_L	0.0025	3.1
27	73% Occipital_Mid_L	1.97E-06	5.9
28	93% Occipital_Mid_L	0.0015	3.3
29	47% Occipital_Sup_L / 32% Cuneus_L	1.29E-06	6.0
30	41% Temporal_Mid_L / 35% Occipital_Mid_L	0.00198	3.2
31	34% Calcarine_L / 26% Occipital_Mid_L	0.00563	2.7
32	67% Calcarine_L	0.00249	3.1
33	45% Precuneus_L / 34% Calcarine_L	3.73E-05	4.7
34	74% Precuneus_L	2.92E-05	4.8
35	46% Precuneus_L / 45% Cingulum_Mid_L	3.02E-05	4.8
NO	**HC Receiving Capacities**	**p-value**	**t-value**
1	45% Frontal_Inf_Tri_R / 28% Frontal_Inf_Orb_R	0.0039	2.8
2	70% Parietal_Sup_R	0.0003	3.8
3	49% Precuneus_R / 40% Cuneus_R	3.05E-12	10.5
4	37% Parietal_Sup_R / 23% Parietal_Inf_R	1.16E-10	9.1
5	80% Precuneus_R	3.72E-15	13.6
6	53% Temporal_Sup_R / 37% SupraMarginal_R	0.0002	3.9
7	46% SupraMarginal_R / 34% Parietal_Inf_R	5.92E-08	6.8
8	87% Angular_R	2.69E-10	8.7

12

9	73% Occipital_Mid_R	3.73E-06	5.3
10	87% Temporal_Mid_R	5.33E-06	5.2
11	64% Temporal_Mid_R	9.73E-06	5.0
12	51% Temporal_Inf_R / 47% Temporal_Mid_R	0.0011	3.3
13	67% Occipital_Mid_R	3.89E-06	5.3
14	42% Occipital_Sup_R / 26% Cuneus_R	5.83E-15	13.4
15	65% Cuneus_R	3.14E-08	7.0
16	37% Occipital_Mid_R / 20% Occipital_Sup_R	0.0063	2.6
17	78% Lingual_R	9.12E-05	4.2
18	39% Calcarine_R / 27% Cuneus_R	6.58E-07	5.9
19	76% Calcarine_R	1.30E-05	4.9
20	44% Cingulum_Post_R / 39% Cingulum_Mid_R	1.94E-15	13.9
21	57% Precuneus_R / 32% Calcarine_R	1.48E-13	11.9
22	42% Cingulum_Mid_R	3.12E-06	5.4
23	79% Precuneus_R	5.16E-15	13.4
24	46% Precuneus_R / 37% Cingulum_Mid_R	1.96E-07	6.4
25	49% Lingual_R / 23% Precuneus_R	0.0001	4.2
26	36% Thalamus_R / 9% Lingual_R	6.38E-05	4.4
27	41% Thalamus_R / 8% Hippocampus_R	0.0105	2.4
28	52% Thalamus_R	2.47E-06	5.5
29	50% Frontal_Sup_Medial_L / 47% Cingulum_Ant_L	0.0010	3.4
30	66% Parietal_Sup_L	2.59E-09	7.9
31	45% Cuneus_L / 40% Precuneus_L	1.76E-11	9.8
32	31% Parietal_Inf_L / 24% Parietal_Sup_L	3.56E-09	7.8
33	75% Precuneus_L	1.11E-16	15.4
34	59% Angular_L / 26% Parietal_Inf_L	1.47E-09	8.1
35	57% Parietal_Inf_L / 36% SupraMarginal_L	0.0005	3.6
36	73% Occipital_Mid_L	0.0001	4.0
37	93% Occipital_Mid_L	4.63E-05	4.5
38	57% Lingual_L / 21% Calcarine_L	0.0063	2.6
39	47% Occipital_Sup_L / 32% Cuneus_L	3.97E-13	11.4
40	88% Lingual_L	4.70E-05	4.5
41	34% Calcarine_L / 26% Occipital_Mid_L	2.57E-05	4.7
42	38% Lingual_L / 20% Calcarine_L	0.0016	3.2
43	67% Calcarine_L	2.24E-05	4.7
44	45% Precuneus_L / 34% Calcarine_L	4.36E-10	8.6
45	39% Cingulum_Mid_L / 22% Cingulum_Post_L	4.69E-14	12.4
46	74% Precuneus_L	1.32E-12	10.9
47	46% Precuneus_L / 45% Cingulum_Mid_L	3.01E-09	7.8
48	55% Cingulum_Post_L / 21% Precuneus_L	0.0012	3.3

13

NO		p-value	t-value
49	53% Thalamus_L	9.34E-05	4.2
NO	**MCS Receiving Capacities**	**p-value**	**t-value**
1	70% Parietal_Sup_R	0.0005	3.7
2	49% Precuneus_R / 40% Cuneus_R	0.0011	3.4
3	37% Parietal_Sup_R / 23% Parietal_Inf_R	0.0002	4.0
4	80% Precuneus_R	6.62E-06	5.4
5	42% Occipital_Sup_R / 26% Cuneus_R	8.88E-06	5.3
6	65% Cuneus_R	0.0011	3.4
7	44% Cingulum_Post_R / 39% Cingulum_Mid_R	0.0002	4.0
8	79% Precuneus_R	4.75E-06	5.5
9	46% Precuneus_R / 37% Cingulum_Mid_R	0.0053	2.8
10	46% Caudate_R / 6% Thalamus_R	0.0051	2.8
11	41% Thalamus_R / 8% Hippocampus_R	0.0001	4.3
12	52% Thalamus_R	3.17E-03	3.0
13	58% Paracentral_Lobule_L / 35% Precuneus_L	0.0038	2.9
14	66% Parietal_Sup_L	5.50E-05	4.6
15	45% Cuneus_L / 40% Precuneus_L	1.20E-05	5.2
16	31% Parietal_Inf_L / 24% Parietal_Sup_L	0.0001	4.3
17	75% Precuneus_L	3.95E-07	6.5
18	59% Angular_L / 26% Parietal_Inf_L	1.45E-05	5.1
19	57% Parietal_Inf_L / 36% SupraMarginal_L	0.0010	3.4
20	47% Occipital_Sup_L / 32% Cuneus_L	2.54E-06	5.8
21	45% Precuneus_L / 34% Calcarine_L	0.0013	3.3
22	39% Cingulum_Mid_L / 22% Cingulum_Post_L	0.0029	3.0
23	74% Precuneus_L	5.03E-06	5.5
24	46% Precuneus_L / 45% Cingulum_Mid_L	0.0006	3.6
25	53% Thalamus_L	0.003	3.0
26	51% Thalamus_L	0.0014	3.3
No	**UWS Receiving Capacities**	**p-value**	**t-value**
1	52% Thalamus_R	0.0001	5.1

1
2
3
4
5
6
7
8
9
10

14

Supplementary Table 4. Group comparison of regional broadcasting and receiving capacities after exogenous perturbations. Brain regional contrasts in broadcasting and receiving capacity between study groups (I.e., UWS vs HC, UWS vs MCS and MCS vs UWS) (Bonferroni corrected p-values <0.05 for 214 tests (ROIs)).

NO	UWS vs HC Broadcasting Capacities	p-value	t-value
1	44% Frontal_Med_VMPFC_R / 31% Cingulum_Ant_R	1.37E-05	-4.9
2	57% Insula_R / 21% Frontal_Inf_Tri_R	5.45E-05	-4.5
3	66% Insula_R	1.72E-07	-6.2
4	56% Insula_R / 24% Rolandic_Oper_R	1.64E-05	-4.8
5	52% Insula_R / 36% Frontal_Inf_Orb_R	8.75E-05	-4.3
6	34% Insula_R / 22% Putamen_R	1.43E-05	-4.9
7	47% Postcentral_R / 23% Parietal_Inf_R	7.82E-05	-4.3
8	57% Rolandic_Oper_R / 34% Insula_R	1.27E-06	-5.6
9	49% Precuneus_R / 40% Cuneus_R	4.43E-06	-5.2
10	37% Parietal_Sup_R / 23% Parietal_Inf_R	0.0002	-4.1
11	53% Temporal_Sup_R / 37% SupraMarginal_R	3.35E-05	-4.6
12	87% Temporal_Mid_R	2.81E-05	-4.7
13	62% Temporal_Pole_Mid_R	3.83E-06	-5.3
14	45% Temporal_Pole_Sup_R / 34% Temporal_Pole_Mid_R	2.21E-07	-6.1
15	58% Temporal_Mid_R / 32% Temporal_Sup_R	2.02E-06	-5.5
16	50% Temporal_Sup_R / 28% Rolandic_Oper_R	4.12E-07	-5.9
17	28% Temporal_Sup_R / 25% Rolandic_Oper_R	2.68E-09	-7.4
18	52% Temporal_Sup_R / 48% Temporal_Mid_R	3.42E-09	-7.3
19	66% Temporal_Mid_R	1.71E-06	-5.5
20	64% Temporal_Mid_R	4.27E-07	-5.9
21	66% Temporal_Inf_R	0.0002	-3.9
22	39% Fusiform_R / 25% Occipital_Inf_R	0.0002	-4.0
23	53% Fusiform_R / 16% Lingual_R	0.0001	-4.1
24	51% Lingual_R / 33% Fusiform_R	7.14E-06	-5.1
25	67% Occipital_Mid_R	0.0002	-4.0
26	42% Occipital_Sup_R / 26% Cuneus_R	0.0001	-4.1
27	48% Lingual_R / 17% Fusiform_R	5.16E-05	-4.5
28	65% Cuneus_R	1.28E-07	-6.3
29	37% Occipital_Mid_R / 20% Occipital_Sup_R	6.34E-05	-4.4
30	78% Lingual_R	2.00E-06	-5.5
31	39% Calcarine_R / 27% Cuneus_R	1.33E-05	-4.9
32	59% Occipital_Inf_R / 23% Lingual_R	4.63E-05	-4.5
33	76% Calcarine_R	1.03E-06	-5.6
34	81% Cingulum_Ant_R	2.82E-06	-5.4

15

35	81% Cingulum_Mid_R	7.24E-06	-5.1
36	57% Precuneus_R / 32% Calcarine_R	2.03E-08	-6.8
37	80% Cingulum_Mid_R	3.14E-06	-5.3
38	46% Precuneus_R / 37% Cingulum_Mid_R	1.23E-06	-5.6
39	28% Amygdala_R / 27% Temporal_Pole_Sup_R	3.22E-06	-5.3
40	36% ParaHippocampal_R / 36% Hippocampus_R	0.0001	-4.2
41	60% ParaHippocampal_R / 28% Fusiform_R	2.82E-05	-4.7
42	49% Lingual_R / 23% Precuneus_R	2.58E-09	-7.4
43	36% Thalamus_R / 9% Lingual_R	0.0001	-4.2
44	52% Thalamus_R	0.0002	-4.0
45	54% Frontal_Med_VMPFC_L / 31% Cingulum_Ant_L	4.43E-05	-4.5
46	46% Frontal_Inf_Orb_L / 36% Insula_L	0.0002	-4.0
47	66% Insula_L	7.43E-06	-5.1
48	52% Cingulum_Mid_L / 45% Supp_Motor_Area_L	0.0001	-4.2
49	37% Temporal_Sup_L / 35% Rolandic_Oper_L	6.28E-05	-4.4
50	59% Insula_L / 23% Rolandic_Oper_L	3.53E-06	-5.3
51	34% Insula_L / 18% Temporal_Sup_L	2.23E-06	-5.4
52	42% Rolandic_Oper_L / 39% Insula_L	1.34E-06	-5.6
53	45% Cuneus_L / 40% Precuneus_L	1.58E-05	-4.8
54	31% Parietal_Inf_L / 24% Parietal_Sup_L	0.0001	-4.2
55	49% Parietal_Inf_L / 38% Postcentral_L	7.43E-06	-5.1
56	44% Temporal_Sup_L / 26% Rolandic_Oper_L	9.18E-08	-6.4
57	40% SupraMarginal_L / 32% Temporal_Sup_L	0.0002	-4.0
58	55% Temporal_Pole_Sup_L / 42% Temporal_Pole_Mid_L	1.17E-06	-5.6
59	57% Temporal_Pole_Mid_L / 25% Temporal_Mid_L	8.93E-06	-5.0
60	54% Temporal_Pole_Sup_L / 27% Temporal_Sup_L	1.08E-08	-7.0
61	62% Temporal_Mid_L	3.51E-07	-6.0
62	82% Temporal_Mid_L	4.51E-05	-4.5
63	72% Temporal_Mid_L	1.08E-09	-7.7
64	71% Fusiform_L	1.03E-05	-5.0
65	73% Occipital_Mid_L	0.0001	-4.2
66	93% Occipital_Mid_L	2.88E-05	-4.7
67	57% Lingual_L / 21% Calcarine_L	1.47E-06	-5.5
68	49% Occipital_Inf_L / 33% Fusiform_L	5.21E-05	-4.5
69	40% Fusiform_L / 31% Lingual_L	8.06E-05	-4.3
70	47% Occipital_Sup_L / 32% Cuneus_L	2.36E-05	-4.7
71	41% Temporal_Mid_L / 35% Occipital_Mid_L	2.73E-08	-6.7
72	49% Occipital_Mid_L / 44% Occipital_Inf_L	7.38E-05	-4.4
73	88% Lingual_L	3.90E-07	-5.9

16

74	34% Calcarine_L / 26% Occipital_Mid_L	0.0002	-4.0
75	38% Lingual_L / 20% Calcarine_L	2.06E-06	-5.4
76	25% Occipital_Inf_L / 23% Lingual_L	2.49E-05	-4.7
77	67% Calcarine_L	4.13E-06	-5.2
78	66% Cingulum_Mid_L	1.28E-05	-4.9
79	50% Cingulum_Ant_L / 39% Frontal_Sup_Medial_L	0.0001	-4.2
80	62% Cingulum_Mid_L	1.99E-06	-5.5
81	37% Cingulum_Mid_L / 36% Cingulum_Ant_L	1.56E-05	-4.8
82	46% Precuneus_L / 45% Cingulum_Mid_L	0.0002	-4.1
83	31% Amygdala_L / 18% Temporal_Pole_Sup_L	5.19E-06	-5.2
84	55% Hippocampus_L / 13% ParaHippocampal_L	4.63E-05	-4.5
85	46% Hippocampus_L / 19% Temporal_Inf_L	6.10E-05	-4.4
86	43% ParaHippocampal_L / 24% Hippocampus_L	2.79E-08	-6.7
87	55% Fusiform_L / 32% ParaHippocampal_L	7.74E-06	-5.1
88	46% Thalamus_L	9.08E-05	-4.3
NO	**MCS vs HC Broadcasting Capacities**	**p-value**	**t-value**
1	66% Insula_R	1.46E-05	-4.7
2	34% Insula_R / 22% Putamen_R	1.89E-05	-4.7
3	62% Temporal_Pole_Mid_R	8.39E-06	-4.9
4	45% Temporal_Pole_Sup_R / 34% Temporal_Pole_Mid_R	1.39E-06	-5.4
5	50% Temporal_Sup_R / 28% Rolandic_Oper_R	0.0002	-3.9
6	28% Temporal_Sup_R / 25% Rolandic_Oper_R	8.42E-07	-5.5
7	52% Temporal_Sup_R / 48% Temporal_Mid_R	0.0001	-4.2
8	66% Temporal_Mid_R	4.80E-07	-5.7
9	64% Temporal_Mid_R	8.23E-05	-4.2
10	66% Temporal_Inf_R	6.94E-05	-4.3
11	39% Fusiform_R / 25% Occipital_Inf_R	0.0002	-4.0
12	53% Fusiform_R / 16% Lingual_R	0.0002	-4.0
13	48% Fusiform_R / 29% Temporal_Inf_R	6.72E-06	-5.0
14	51% Lingual_R / 33% Fusiform_R	0.0002	-3.9
15	76% Calcarine_R	0.0002	-4.0
16	60% ParaHippocampal_R / 28% Fusiform_R	4.70E-05	-4.4
17	49% Lingual_R / 23% Precuneus_R	7.02E-05	-4.3
18	36% Thalamus_R / 9% Lingual_R	3.19E-06	-5.2
19	52% Thalamus_R	1.18E-06	-5.4
20	34% Insula_L / 18% Temporal_Sup_L	6.16E-06	-5.0
21	71% Fusiform_L	5.45E-05	-4.4
22	57% Lingual_L / 21% Calcarine_L	0.0002	-4.0
23	88% Lingual_L	6.04E-05	-4.3

17

24	55% Hippocampus_L / 13% ParaHippocampal_L	0.0002	-3.9
25	43% ParaHippocampal_L / 24% Hippocampus_L	0.0001	-4.2
26	55% Fusiform_L / 32% ParaHippocampal_L	0.0001	-4.1
27	46% Thalamus_L / 1% Lingual_L	4.53E-08	-6.3
NO	**MCS vs UWS Broadcasting Capacities**	**p-value**	**t-value**
1	70% Parietal_Sup_R	0.0001	-4.3
2	54% Temporal_Pole_Sup_L / 27% Temporal_Sup_L	0.0002	-4.0

1

NO	UWS vs HC Receiving Capacities	t-value	p-value
1	44% Frontal_Med_VMPFC_R / 31% Cingulum_Ant_R	0.0002	-4.1
2	49% Precuneus_R / 40% Cuneus_R	7.27E-08	-6.4
3	37% Parietal_Sup_R / 23% Parietal_Inf_R	1.37E-05	-4.9
4	80% Precuneus_R	9.12E-10	-7.7
5	87% Angular_R	0.0002	-4.0
6	58% Temporal_Mid_R / 32% Temporal_Sup_R	0.0002	-4.0
7	50% Temporal_Sup_R / 28% Rolandic_Oper_R	0.0002	-4.1
8	52% Temporal_Sup_R / 48% Temporal_Mid_R	6.08E-06	-5.1
9	64% Temporal_Mid_R	2.21E-06	-5.4
10	67% Occipital_Mid_R	8.68E-05	-4.3
11	42% Occipital_Sup_R / 26% Cuneus_R	1.31E-07	-6.3
12	65% Cuneus_R	2.96E-06	-5.3
13	37% Occipital_Mid_R / 20% Occipital_Sup_R	0.0002	-4.0
14	78% Lingual_R	0.0002	-4.0
15	39% Calcarine_R / 27% Cuneus_R	1.64E-05	-4.8
16	76% Calcarine_R	3.30E-05	-4.6
17	81% Cingulum_Ant_R	0.0002	-3.9
18	44% Cingulum_Post_R / 39% Cingulum_Mid_R	5.94E-10	-7.8
19	57% Precuneus_R / 32% Calcarine_R	1.02E-12	-9.8
20	42% Cingulum_Mid_R	5.51E-06	-5.2
21	79% Precuneus_R	9.03E-10	-7.7
22	46% Precuneus_R / 37% Cingulum_Mid_R	2.07E-08	-6.8
23	49% Lingual_R / 23% Precuneus_R	2.95E-05	-4.6
24	54% Frontal_Med_VMPFC_L / 31% Cingulum_Ant_L	6.84E-05	-4.4
25	50% Frontal_Sup_Medial_L / 47% Cingulum_Ant_L	1.98E-06	-5.5
26	52% Frontal_Inf_Tri_L / 42% Frontal_Inf_Oper_L	0.0001	-4.2
27	50% Precentral_L / 30% Frontal_Inf_Oper_L	0.0002	-4.1
28	68% Postcentral_L	0.0002	-4.0
29	66% Parietal_Sup_L	9.90E-09	-7.0
30	45% Cuneus_L / 40% Precuneus_L	4.66E-07	-5.9
31	31% Parietal_Inf_L / 24% Parietal_Sup_L	8.11E-08	-6.4
32	75% Precuneus_L	2.72E-12	-9.5

18

33	49% Parietal_Inf_L / 38% Postcentral_L	0.0001	-4.3
34	59% Angular_L / 26% Parietal_Inf_L	1.16E-06	-5.6
35	57% Parietal_Inf_L / 36% SupraMarginal_L	0.0001	-4.2
36	48% Temporal_Inf_L / 46% Temporal_Mid_L	0.0002	-4.0
37	73% Occipital_Mid_L	0.0002	-4.0
38	93% Occipital_Mid_L	3.79E-05	-4.6
39	57% Lingual_L / 21% Calcarine_L	0.0001	-4.2
40	47% Occipital_Sup_L / 32% Cuneus_L	2.25E-10	-8.1
41	41% Temporal_Mid_L / 35% Occipital_Mid_L	1.41E-05	-4.9
42	88% Lingual_L	7.38E-05	-4.4
43	34% Calcarine_L / 26% Occipital_Mid_L	4.65E-05	-4.5
44	67% Calcarine_L	0.0001	-4.2
45	62% Cingulum_Mid_L	0.0001	-4.2
46	37% Cingulum_Mid_L / 36% Cingulum_Ant_L	0.0002	-4.1
47	45% Precuneus_L / 34% Calcarine_L	3.14E-08	-6.7
48	39% Cingulum_Mid_L / 22% Cingulum_Post_L	3.82E-12	-9.4
49	74% Precuneus_L	1.62E-09	-7.5
50	46% Precuneus_L / 45% Cingulum_Mid_L	2.67E-08	-6.7
NO	**MCS vs HC Receiving Capacities**	**p-value**	**t-value**
1	64% Temporal_Mid_R	3.17E-05	-4.5
2	78% Lingual_R	0.0002	-3.9
3	39% Calcarine_R / 27% Cuneus_R	5.91E-05	-4.3
4	44% Cingulum_Post_R / 39% Cingulum_Mid_R	1.26E-05	-4.8
5	57% Precuneus_R / 32% Calcarine_R	1.39E-06	-5.4
6	79% Precuneus_R	3.58E-05	-4.5
7	45% Cuneus_L / 40% Precuneus_L	3.01E-05	-4.5
8	45% Precuneus_L / 34% Calcarine_L	5.78E-06	-5.0
9	39% Cingulum_Mid_L / 22% Cingulum_Post_L	2.96E-07	-5.8
10	74% Precuneus_L	8.44E-05	-4.2
NO	**MCS vs UWS Receiving Capacities**	**p-value**	**t-value**
1	75% Precuneus_L	0.0002	-4.1
2	47% Occipital_Sup_L / 32% Cuneus_L	9.29E-05	-4.4
3	74% Precuneus_L	0.0002	-4.0

1

Neural mechanisms behind loss of consciousness following brain injury are still unclear. We quantify them through casual neural interactions after spontaneous perturbation and In-silico exogenous perturbations. Impaired posterior integration and thalamo-frontotemporal broadcasting characterize disorders of consciousness.